

Accepted Manuscript

Research papers

Biophysical flocculation of suspended particulate matters in Belgian coastal zones

Xiaoteng Shen, Erik A. Toorman, Byung Joon Lee, Michael Fettweis

PII: S0022-1694(18)30789-3

DOI: <https://doi.org/10.1016/j.jhydrol.2018.10.028>

Reference: HYDROL 23192

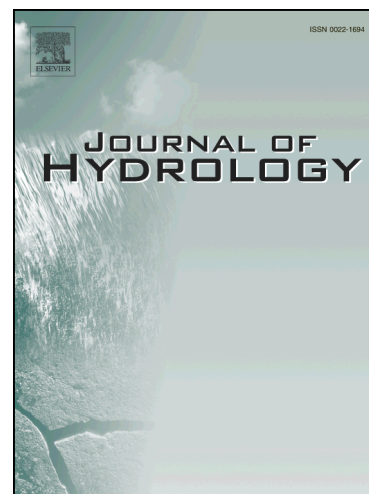
To appear in: *Journal of Hydrology*

Received Date: 24 September 2018

Accepted Date: 12 October 2018

Please cite this article as: Shen, X., Toorman, E.A., Joon Lee, B., Fettweis, M., Biophysical flocculation of suspended particulate matters in Belgian coastal zones, *Journal of Hydrology* (2018), doi: <https://doi.org/10.1016/j.jhydrol.2018.10.028>

This is a PDF file of an unedited manuscript that has been accepted for publication. As a service to our customers we are providing this early version of the manuscript. The manuscript will undergo copyediting, typesetting, and review of the resulting proof before it is published in its final form. Please note that during the production process errors may be discovered which could affect the content, and all legal disclaimers that apply to the journal pertain.



Biophysical flocculation of suspended particulate matters in Belgian coastal zones

Xiaoteng Shen ^{a,*}, Erik A. Toorman ^a, Byung Joon Lee ^b, Michael Fettweis ^c

^a *Hydraulics Laboratory, Department of Civil Engineering, Katholieke Universiteit Leuven, Kasteelpark Arenberg 40, B-3001 Leuven, Belgium*

^b *School of Construction and Environmental Engineering, Kyungpook National University, 2559 Gyeongsang-daero, Sangju, Gyeongbuk 742-711, Korea*

^c *Operational Directorate Natural Environment, Royal Belgian Institute of Natural Sciences, Rue Vautier 29, 1000 Brussels, Belgium*

Abstract

The Flocculation Size Distributions (FSDs) of biomineral suspended particles are of great importance to understand the dynamics of bio-mediated Suspended Particulate Matters (SPMs). Field observations were investigated at Station MOW1 in Belgian coastal waters (southern North Sea) during two typical periods with abundant and reduced biomass. In addition, the Shen et al. (2018) [Water Res. Vol 145, pp 473-486] multi-class population balance flocculation model was extended to address the occurrence of suspended microflocs, macroflocs and megaflocs during these contrasting periods. The microflocs are treated as elementary particles that constitute macroflocs or megaflocs. The FSD is represented by the size and mass fraction of each particle group, which corresponds to a temporal and spatial varying mass weighted settling velocity. The representative sizes of macroflocs and megaflocs are unfixed and migrated between classes mainly due to the effects of turbulent shear, differential settling and biofilm growth. The growth of an aggregate because of bio-activities is allotted to each elementary particle. It is further

* Corresponding author. Hydraulics Laboratory, Department of Civil Engineering, Katholieke Universiteit Leuven, Kasteelpark Arenberg 40, B-3001 Leuven, Belgium.

E-mail addresses: xiaoteng.shen@kuleuven.be (X. Shen).

hypothesized that the growth kinetics of biomineral particles due to biofilm coating follows the logistic equation. This simple bio-flocculation model has been successfully coupled in the open source TELEMAC modeling system with five passive tracers in a quasi-1D vertical case. Within an intra-tide scale, the settling velocity (w_s) is large during slack tides while it is small during maximum current velocities because of variations in turbulence intensities. Nonetheless, the w_s may be largely underestimated when the biological effect is neglected. For a seasonal pattern, the w_s is higher in biomass-rich periods in May than in biomass-poor periods in October. While the mean sizes of megaflocs are close during the two periods, the macroflocs during algae bloom periods are more abundant with a larger mean size. This study enhances our knowledge on the dynamics of SPMs, especially the biophysical influences on the fate and transport of estuarine aggregates.

Keywords: Population balance model; flocculation; floc size distribution; biofilm growth; suspended particulate matter; Belgian coast

1. Introduction

In recent years considerable attention has been paid to the dynamics and the biogeochemical functions of Suspended Particulate Matter (SPM) along the cross-shore gradient, from the coastal zone to the outer continental shelf as well as in the whole land-shelf-ocean interaction areas, because of the major role it plays in morphodynamical and ecosystem functioning (Maerz et al., 2016; Markussen et al., 2016; Yu et al., 2016; Shchepetkina et al., 2017; Li et al., 2017; Lee et al., 2017; Fettweis and Lee, 2017). For instance, SPM dynamics

strongly influences the formation of the turbidity maxima in estuaries and coastal zones (e.g., Uncles et al., 2006; Fettweis et al., 2014; Kitheka et al., 2016), and the dredging management in silted harbors and navigational channels (e.g., Van Maren et al., 2009; De Jonge et al., 2014; Fettweis et al., 2016). Besides, the SPM absorbs and scatters light, which contributes to the water clarity and the penetration depth of light; therefore, it is a critical parameter influencing the primary production (Capuzzo et al., 2015). Moreover, pollutants such as heavy metals or polychlorinated biphenyls can be transported with contaminated sediments (e.g., Demirak et al., 2012; Montuori et al., 2016) and impact both deposit-feeding and filter-feeding animals that live by consuming the organic material colonized in the aggregates (Andersen and Pejrup, 2011).

SPM occurs as dense or fluffy flocs mostly with size in the magnitude range of micrometers to millimeters, with a few exceptions of larger “marine snow” particles. The flocs can settle to the bed of the water column since the settling flux and the deposition rates of the flocs are largely modified compared to that of primary particles. In natural environments, flocs can be divided into inorganic and organic components (Droppo, 2001; Maggi, 2009). The inorganic component consists of clays (such as kaolinite, montmorillonite, illite and chlorite) and other minerals (such as quartz and carbonates), while the organic component is composed of microorganisms and their metabolic products. Although various laboratory studies address the inorganic flocs (Maggi, 2005; Tang et al., 2014; Keyvani and Strom, 2014; Shen and Maa, 2016a, 2017; Tran and Strom, 2017), in-situ observations show that a floc is actually a micro-ecosystem preferable for microorganism colonization and biofilm formation (Droppo et al., 1997; Droppo, 2001; Tang and Maggi, 2016; Tang, 2017; Fang et al., 2017; Chen et al., 2017), with inorganic particles coated with various organic matters such as fecal pellets and different phytoplankton cells (Riebesell, 1991; Edolvang and Austen, 1997). The organic component is involved in

various biological activities that may enhance the aggregation by, for example, secretion of carbohydrates or production of fecal pellets and pseudo-feces that may increase the stickiness of the SPM (Passow et al., 2001; Fugate and Friedrichs, 2002; Andersen and Pejrup, 2011). Phytoplankton blooms in turbid areas interact with the inorganic particles and may increase the aggregation and thus leading to the formation of megaflocs (Thornton, 2002; Fettweis et al., 2014; Fettweis and Baeye, 2015; Playter et al., 2017; Fettweis and Lee, 2017). The inorganic or organic particles are biologically glued by polymeric fibrils (Liss et al., 1996), which are named as Extracellular Polymeric Substance (EPS) or Transparent Exopolymer Particles (TEP; Alldredge et al., 1993). In reality, the term EPS is broader than TEP, and refers to any extracellular dissolved organic matter released by prokaryotes or eukaryotes (Bar-Zeev et al., 2015). EPS are mainly made up of a fraction of soluble carbohydrates composed of galactose and glucuronic acid, but also made up of a particle fraction in the form of TEP (Morelle et al., 2017). In other words, TEP is a subgroup of EPS that is exuded by bacteria or some microalgae that can promote biofilm formation (Thornton, 2002; Bhaskar and Bhosle, 2005; Bar-Zeev et al., 2015; Discart, 2015). These biological activities are highlighted in interpreting the SPM dynamics (Tang, 2017), and are of comparable importance with other physical (e.g., turbulent shear and SPM concentration) and chemical (e.g., salinity, PH and ionic strength) parameters.

In order to accurately estimate the fate and transport of SPM, various optical and acoustic approaches are used to highlight the SPM concentration and the Floc Size Distributions (FSDs). The signals of optical instrument such as OBS (Optical Backscatter Sensor) can be calibrated to reflect the SPM concentration. On the other hand, acoustic instruments such as ADV (Acoustic Doppler Velocimeter) or ADCP (Acoustic Doppler Current Profiler) can be used to convert acoustic backscatter into SPM concentration. Nevertheless, these sensor derived SPM

concentrations have uncertainties that are associated with the flocculation dynamics of the particles (Rouhnia et al., 2014; Vincent and MacDonald, 2015; Shao and Maa, 2017), which underlines the importance of measuring FSDs in order to investigate various sediment properties. Nowadays, the measurements of FSDs have greatly improved by modern optical techniques. For instance, the LISST (Laser In Situ Scattering and Transmissometry) instrument is widely used to acquire FSDs with 32 size groups with its transmission sensors (e.g., Shao et al., 2011; Fettweis et al., 2014; Guo et al., 2017), and various expensive or inexpensive camera systems are also developed to process FSDs with an image processing software (e.g., Maggi et al., 2006; Smith and Friedrichs, 2011, 2015; Keyvani and Strom, 2014; Shen and Maa, 2016a). Recently, a combination of both LISST and camera system has been applied in the York River (Cartwright, 2013) to achieve FSDs with wider size ranges. Nevertheless, camera systems are limited to low turbidity and low current velocities (Winter et al., 2007), and thus, they are difficult to apply in regions such as Changjiang (Yangtze) River Estuary of China with relatively high sediment concentrations and large currents (Shao et al., 2017).

Mathematical models are another practical tool to interpret the SPM dynamics and test various particle collision mechanisms. Some models are based on Lattice Boltzmann simulation (Zhang and Zhang, 2011; Zhang et al., 2013, 2016), which, however, up to date have not been applied to large study domains or included biological effects. Some models predict the mean floc size responding to selected environmental variables (such as SPM, shear rate, temperature and salinity) using the artificial neural network through data training (e.g., Sahin et al., 2017). However, these approaches treat the flocculation mechanisms as a black box and fail to explain why and how the network structure should be the one as claimed. Besides these work, most flocculation models that have been proposed are based on the expansion of early work by

Smoluchowski (1917) for pure aggregation processes (Thomas et al., 1999). By adding breakage terms, Winterwerp (1998)'s Lagrangean flocculation model and its variants are widely used to describe the aggregation and breakage of suspended clays in estuaries. Based on this model, Maggi (2009) separated the floc solid volume into mineral and biomass fractions, which is among the earliest bio-flocculation models to examine SPM dynamics in coastal zones and estuaries. There are some weak points and lacuna in that model. Firstly, the consideration of only one floc size (usually the median size) may increase the uncertainties when multimodal FSDs occur. Secondly, only the effect of turbulent shear is included, while differential settling may also be crucial during slack tide when the turbulence is reduced (Eisma, 1991; Lick et al., 1993). Besides, the impact of seasonal bio-activities on floc size is ignored in Maggi's model. The first two deficiencies can be overcome by using the population balance modeling either to better display the entire FSD with multi-size groups (e.g., Zhang and Li, 2003; Nopens, 2005; Maggi et al., 2007; Shen and Maa, 2015, 2016b; Shen, 2016), or to better address the computational efficiency with only two or three classes (e.g., Lee et al., 2011, 2014; Shen et al., 2018). Similar approaches can also be applied in purely organic aggregates during algae bloom period (Jackson, 1990; Jackson and Burd, 2015). The third weakness can be improved by implementing seasonal variations in flocculation parameters, such as floc strength or flocculation efficiency (Chen et al., 2018). So far a biological multi-class flocculation model that can be implemented in open source modeling systems for biomineral aggregates is still not available.

The objective of this study is to fill the scientific gaps about the bio-mediated flocculation of suspended sediments and its impacts on SPM dynamics during biomass-rich and biomass-poor periods. To achieve this target, field observations have been used from the Belgian coastal region (southern North Sea) to investigate the FSDs and SPM concentrations in a typical

shallow, well-mixed coastal zone with high SPM concentration and high hydrodynamic energy (Van den Eynde and Fettweis, 2006). The existing Shen et al. (2018) three-class flocculation model is extended to incorporate biomineral flocs and is applied to the southern North Sea. This new model allows the tracking of size-varying megaflocs, as it includes a simple mechanism to incorporate the sediment particles coated with biofilms and is crucial in enhancing the predictability of particle dynamics in natural and anthropogenic impacted estuarine and coastal systems.

2. Study area and data analysis

The study region is the Belgian nearshore area situated in the southern North Sea (Fig. 1). This area is shallow with a water depth of about 10 m at spring and is characterized by the occurrence of a coastal turbidity maximum (Fettweis et al., 2006, 2016). The SPM concentration at the surface belongs between 20 and 250 mg/L, while near the bed it varies from 100 mg/L to more than a few g/L (Fettweis et al., 2014; Fettweis and Lee, 2017). The port of Zeebrugge is located in the center of the turbidity maximum zone and is subject to heavy siltation. An average of 4×10^6 ton of sediment is dredged annually by the Flemish Government to maintain the navigational depth in the port. The area near Zeebrugge is tidally dominated, and the semi-diurnal tides have a mean tidal range of 2.8 m (neap tide) - 4.3 m (spring tide). The nearshore tidal current ellipses are elongated and vary on average between 0.2 and 0.8 m/s during spring tide and 0.2 and 0.5 m/s during neap tide at 2 m above the bed. In general, the water column at this region is well-mixed due to strong tidal currents but low freshwater discharges.

Southwesterly winds dominate the overall wind climate, followed by winds from the NE sector. Maximum wind speeds coincide with southwesterly winds; nevertheless, the highest waves are

generated under northwesterly winds, due to a longer fetch. The waves have generally a period of about 4 s, lower frequency swell waves with a period of about 6 s are less abundant. The median significant wave height is 0.6 m and the P90 percentile is 1.2 m (Baeye et al., 2011). The temperature of sea water varies from about 3°C in February-March to 20°C in August. Salinity is generally between 28 to 34 ppt, varying mainly due to the advection of water mass exchanging between the Scheldt, Rhine and Seine and the ocean (Arndt et al., 2011; Fettweis and Baeye, 2015). The sources of present-day SPM are mainly from the erosion and resuspension of the Holocene and recent mud deposits that outcrop in the Belgian nearshore area (Adriaens et al., 2018).

Data of current velocity, salinity, SPM concentration and FSD were collected in 2013 with tripods at the station MOW1 (51° 21.63' N, 3° 7.41' E, 5 km offshore and close to Zeebrugge, as shown in Fig. 1). Previous studies clearly show a seasonal variation of SPM concentration, floc size and density, and floc settling velocity. This annual cycle is caused by the seasonal biological cycle, rather than winds or waves (Fettweis et al., 2014; Fettweis and Lee, 2017). The chlorophyll *a* concentration (Chl *a*) is often used as an estimate of algae biomass (Stanley et al. 2003). A dataset from MODIS (Moderate Resolution Imaging Spectroradiometer) satellite was used to analyze the annual Chl *a* concentrations in 2013 at station MOW1 (Fig. 2). The peak Chl *a* concentration (19.1 µg/L) occurred on May 8th (Julian day 128 in the year 2013, two days before spring tide). This period is selected to address the effects of bio-activities on flocculation. A second bloom (summer bloom) occurred on August 18th with Chl *a* concentration reaching 7.6 µg/L. The bio-activity is low between fall and early spring with Chl *a* concentration less than 3.0 µg/L. A day in fall (October 10th, Julian day 280) is selected to represent a typical biomass-poor period for comparison. Chl *a* concentration together with PON

(Particulate Organic Nitrogen), POC (Particulate Organic Carbon) and SPM concentration are also available from in situ water samples taken hourly during about four tidal cycles (13 samples per tidal cycle) a year. The samples for POC, PON and SPM are filtered on board using pre-weighed glass fiber filters and analyzed in the laboratory by element analysis or gravimetric weighing, respectively. Chl *a* concentration is filtered on glass fiber filters, stored in liquid Nitrogen and determined in the lab using spectrophotometry. All our POC/SPM (50 tidal cycles from 2004-2018) and Chl *a* (26 cycles from 2002-2003 and from 2012-2018) data are compiled into Fig. 3 prior to averaging the values over the tidal cycle, because it represents a good ‘climatological’ overview. As shown in Fig. 3, Chl *a* concentration is high between March and September but low during winter, and the spring bloom peak is clearly visible. For the POC content in the SPM, the values are similar during whole the year, except during the spring bloom when the POC content also increases. During the sampling year 2013, the ratio of POC/SPM, an indicator of the total organic content (Fettweis et al., 2006; Fettweis and Lee, 2017), is more or less a constant. Thus, the mean value of $\text{POC/SPM} = 0.047$ is used during the study period, which agrees with Maggi (2009) who suggest a value of 0.04 for the same area. The mean value of the ratio PON/POC is 0.13 ± 0.01 , close to the Redfield ratio of $\text{N:C} = 16:106$ (Redfield, 1934).

Deployments of tripod measurements cover the above period of interest. The instrumentation attached to the tripod consisted of two D&A OBSs, a SonTek 5 MHz ADV Ocean and a Sequoia LISST-100C. The OBSs, ADV and LISST are averaged every 10 or 15 min. The two OBSs measure the SPM concentration at 0.2 m and 2 m above the bed (hereafter referred to as mab). The ADV measures the flow velocity and turbulence close to the bed (around 0.2 mab). The turbulent kinetic energy and thus the shear velocity u^* are derived from

the ADV (Sherwood et al., 2006). The LISST was mounted at 2 mab. It measures the volume concentrations of each size class to constitute the FSDs, and thus the median size D_{50} and Total Volume Concentration (TVC) can be computed from the FSDs. The optical transmission can also be achieved from LISST to evaluate the data quality. Smooth (i.e., no sudden decrease) optical transmission within a range between 0.15-0.98 indicates good quality data. The measured FSDs are decomposed into four lognormal distributions using software DistFit (Chimera Technologies in USA, see Lee et al., 2012):

$$\frac{dV}{dD} = \sum_{i=1}^4 \frac{\bar{V}_i}{\sqrt{2\pi} \ln(\sigma_i)} \exp \left[-\frac{1}{2} \left(\frac{\ln(D/\bar{D}_i)}{\ln(\sigma_i)} \right)^2 \right] \quad (1)$$

where D and V are the size classes and the corresponding volume concentrations reported in LISST, and \bar{D}_i , σ_i and \bar{V}_i are the representative sizes, standard deviations and volumetric concentrations of i th lognormal FSD for primary particles, microflocs, macroflocs and megaflocs, respectively. The primary particles are merged into the microflocs to represent three size classes that coincide with the model assumption (Shen et al., 2018). The measured settling velocities are computed based on the above decomposition (Lee et al., 2012) or estimated by a combination of LISST and sampling results (Markussen and Andersen, 2013). The temperature was 10 °C and the salinity was 30 ppt during the peak Chl a period.

3. Model description

3.1 Flocculation model

Shen et al. (2018) have successfully coupled a three-class population balance model in the open TELEMAC system for mineral cohesive particles. Nevertheless, in a natural environment, the aggregates are, during periods with high primary production, also coated with

biofilms due to EPS or TEP binding. By assuming that the macroflocs and megaflocs are composed of elementary microflocs, the enlarged floc size attributed to biofilm attachment can be averaged to each elementary microfloc (Fig. 4). The microflocs may be in suspension, or presented as part of macroflocs or megaflocs. A floc can be generated because of aggregation of smaller particles or breakage of larger flocs, with additional size increase because of biofilm attachment. A total of five tracers are tracked in this model: (1) N_P – number density of microflocs (i.e., number of microflocs per unit fluid volume) only in suspension, (2) N_{F1} – number density of macroflocs in suspension, (3) N_{T1} – number of microflocs in macroflocs (per unit fluid volume), (4) N_{F2} – number density of megaflocs in suspension, and (5) N_{T2} – number of microflocs in megaflocs (per unit fluid volume). Based on the above definition, the average number of microflocs in one macrofloc N_{C1} or megafloc N_{C2} at each time step can be computed as:

$$\begin{cases} N_{C1} = N_{T1} / N_{F1} \\ N_{C2} = N_{T2} / N_{F2} \end{cases} \quad (2)$$

As a consequence, the sizes of macroflocs D_{F1} and megaflocs D_{F2} can be written as:

$$\begin{cases} D_{F1} = D_P \cdot N_{C1}^{1/n_f} \\ D_{F2} = D_P \cdot N_{C2}^{1/n_f} \end{cases} \quad (3)$$

where n_f is the mean fractal dimension of flocs. Different from the previous model (Shen et al., 2018), the size of megaflocs D_{F2} are varied in this study, since a constant D_{F2} may only be valid during a short period.

The mass fraction of microflocs m_P , macroflocs m_{F1} and megaflocs m_{F2} follows:

$$\begin{cases} m_P = N_P / (N_P + N_{T1} + N_{T2}) \\ m_{F1} = N_{T1} / (N_P + N_{T1} + N_{T2}) \\ m_{F2} = N_{T2} / (N_P + N_{T1} + N_{T2}) \end{cases} \quad (4)$$

Both (i) aggregation and breakage due to two-body collisions and (ii) floc growth due to biofilm attachment are considered in our model. Similar to that shown in Shen et al. (2018), six aggregations and two breakages processes are explicitly addressed (Table 1). Without the assumption of size-fixed megaflocs, the tracer N_{F2} becomes independent in the model. Among all aggregation processes, the collision of a microfloc and a microfloc/macrofloc/megafloc, and the collision of a macrofloc and a megafloc will not alter the number of megaflocs (N_{F2}) in suspension. Instead, the collision of two macroflocs leads to an increase in number of $\frac{1}{2} \left(\frac{1}{N_{C2}/N_{C1}-1} \right)$ megaflocs, while the collision of two megaflocs leads N_{F2} decreased by half. Notice that the former is similar to the treatment for collision of two microflocs, distributing the stoichiometric number based on the mass fraction (Lee et al., 2011; Shen et al., 2018). The breakage of a macrofloc will not influence N_{F2} , while the breakage of a megafloc will make this megafloc disappear. As a result, the source and sink terms for the above five tracers for six aggregation and two breakage processes can be summarized as:

$$S_p = -\frac{1}{2} \alpha \beta_{pp} N_p N_p \left(\frac{N_{C1}}{N_{C1}-1} \right) - \alpha \beta_{PF1} N_p N_{F1} - \alpha \beta_{PF2} N_p N_{F2} + f_{P1} N_{C1} a_{F1} N_{F1} + f_{P2} N_{C2} a_{F2} N_{F2} \quad (5a)$$

$$S_{F1} = \frac{1}{2} \alpha \beta_{pp} N_p N_p \left(\frac{1}{N_{C1}-1} \right) - \frac{1}{2} \alpha \beta_{F1F1} N_{F1} N_{F1} \left(\frac{N_{C2}/N_{C1}}{N_{C2}/N_{C1}-1} \right) - \alpha \beta_{F1F2} N_{F1} N_{F2} + (K_1 - 1) a_{F1} N_{F1} + K_2 a_{F2} N_{F2} \quad (5b)$$

$$S_{T1} = \frac{1}{2} \alpha \beta_{pp} N_p N_p \left(\frac{N_{C1}}{N_{C1}-1} \right) + \alpha \beta_{PF1} N_p N_{F1} - \frac{1}{2} \alpha \beta_{F1F1} N_{F1} N_{F1} \left(\frac{N_{C2}}{N_{C2}/N_{C1}-1} \right) - N_{C1} \alpha \beta_{F1F2} N_{F1} N_{F2} - f_{P1} \cdot N_{C1} a_{F1} N_{F1} + (1 - f_{P2}) \cdot N_{C2} a_{F2} N_{F2} \quad (5c)$$

$$S_{F_2} = \frac{1}{2} \alpha \beta_{F_1 F_1} N_{F_1} N_{F_1} \left(\frac{1}{N_{C_2} / N_{C_1} - 1} \right) - \frac{1}{2} \alpha \beta_{F_2 F_2} N_{F_2} N_{F_2} - a_{F_2} N_{F_2} \quad (5d)$$

$$S_{T_2} = \alpha \beta_{P F_2} N_P N_{F_2} + \frac{1}{2} \alpha \beta_{F_1 F_1} N_{F_1} N_{F_1} \left(\frac{N_{C_2}}{N_{C_2} / N_{C_1} - 1} \right) + N_{C_1} \alpha \beta_{F_1 F_2} N_{F_1} N_{F_2} - N_{C_2} a_{F_2} N_{F_2} \quad (5e)$$

These equations also include an assumption for the fragmentation distribution function (Maggi et al., 2007; Shen and Maa, 2015) which represents the FSDs of daughter particles produced by the breakage of a parent particle. When a macrofloc breaks up, f_{P1} percentage of its mass will release microflocs while the rest will tear into number of K_1 macroflocs (Process 7 in Table 1); similarly, when a megafloc breaks up, f_{P2} percentage of its mass will create microflocs while the rest will split into number of K_2 macroflocs (Process 8 in Table 1). In Eq. 5, α is the collision efficiency. In some of the literature this parameter was calculated with more complicated formula (e.g., Maggi, 2007; Zhang et al., 2016). However, none of them are widely accepted to account for the forces and the biofilm induced stickiness for environmental sediments. Thus, α is treated here as a fitting constant for simplicity, following previous work by Verney et al. (2010), Lee et al. (2011, 2014) and Shen and Maa (2015).

The collision frequency β contains the linear effect of turbulent shear, differential settling and Brownian motion (Smoluchowski, 1917; Camp and Stein, 1943; Maggi, 2005; Shen and Maa, 2015):

$$\beta_{ij} = \frac{1}{6} (D_i + D_j)^3 G_\varepsilon + \frac{\pi}{4} (D_i + D_j)^2 |w_{s,i} - w_{s,j}| + \frac{2K_B T}{3\mu} \left(\frac{1}{D_i} + \frac{1}{D_j} \right) (D_i + D_j) \quad (i, j = P, F1, F2) \quad (6)$$

where G_ε is the shear rate that can be calculated by a hydrodynamic model, K_B is the Boltzmann constant, T is the Kelvin temperature, μ is the dynamic viscosity of the fluid and w_s is the settling velocity of the flocs. Although the effect of Brownian motion is small for flocs in estuaries, it is

included in Eq. 6 for a complete expression. The effects of differential settling and turbulent shear may not be omitted on an intra-tidal scale.

The breakage frequency a_F for macroflocs or megaflocs can be written as (Winterwerp, 1998):

$$a_{Fi} = E_b \cdot G_\varepsilon \cdot \left(\frac{D_{Fi} - D_P}{D_P} \right)^{3-nf} \cdot \left(\frac{\mu G_\varepsilon}{F_y / D_{Fi}^2} \right)^{1/2} \quad (i = 1, 2) \quad (7)$$

where E_b is the breakage fitting parameter and F_y is the floc strength.

Our model assumes that the biofilm growth of macroflocs or megaflocs is averaged to the growth of its elementary microflocs. It is further hypothesized that the particle/floc growth kinetics are similar to microbial growth kinetics except with different growth rates. Thus, the growth of a microfloc due to biofilm glue can be modeled as the logistic equation (Maggi, 2009):

$$\frac{\partial D_P}{\partial t} = r_B \cdot D_P \cdot \left(1 - \frac{D_P}{K} \right) \quad (8)$$

where r_B is nutrient dependent growth rate of biomass (s^{-1}) and K is the carrying capacity of microflocs (m). It is critical to note that Eq. 8 is only valid for seasons with high light availability. The growth rate of biomass is, in case of sufficient nutrients, mainly related to the light intensity such as in the North Sea. In other words, in winter when the primary production is low, r_B may be set to null even when the nutrient concentration is high, in order to reproduce seasonality in floc size.

The carrying capacity K can be logically expressed as:

$$K = \gamma_F \cdot (1 + \Omega) \cdot \eta_{Kol} / N_{C2} \quad (9)$$

where γ_F is a fitting constant and the parameter $\Omega = \text{POC}/\text{SPM}$ represents the biomass fraction in SPM. In reality, the POC incorporates the preserved or refractory fraction of the organic matter, and the labile fraction that is associated with the seasonal formation and decay of fresh organic

matter by algae bloom and bacterial activity (Ittekkot, 1988; Keil et al., 1994). The Chlorophyll data could be a proxy for the labile fraction of POC, before detailed analyses of TEP samples are available.

The Kolmogorov micro-length scale η_{Kol} in Eq. 9, which is the smallest scale in the turbulent flow field at which dissipation takes place (Winterwerp and van Kesteren, 2004), controls the ultimate floc size under biomass-poor conditions (Keyvani and Strom, 2014; Van Leussen, 1988):

$$\eta_{Kol} = \left(\frac{\nu}{G_\varepsilon} \right)^{\frac{1}{2}} \quad (10)$$

in which ν is the molecular kinematic viscosity and G_ε is the shear rate. Thus, the meaning of η_{Kol}/N_{C2} is the turbulence induced maximum size of microflocs. The existence of biomass increases the possible maximum size, and therefore the factor $(1+\Omega)$ has taken into account the increase in particle size due to enhanced cohesiveness because of bio-activities (Maggi, 2009). Notice that although it is often written that the Kolmogorov scale limits the size of flocs, we could imagine that the breakage of a floc also depends on its strength, which indicates that strong flocs may survive from an eddy of the same size. A better correlation between K and the maximum floc size should be improved in the future.

The sinking of relatively compact microflocs is assumed following the Stokes law, while the settling velocity of macroflocs or megaflocs is applied in the model by modifying the Stokes equation (Winterwerp, 1998; Lee et al., 2014; Shen et al., 2018):

$$w_{s,Fi} = (1 - \Phi)^A \cdot \frac{1}{18} \frac{(\rho_P - \rho_w)g}{\mu} D_P^{3-n_f} \frac{D_{Fi}^{n_f-1}}{1+0.15Re_i^{0.687}} \quad (11)$$

where Φ is the particle volume fraction, A is an empirical parameter in the range 2.5 to 5.5 (Richardson and Zaki, 1954), ρ_P is the density of constituting particles, ρ_w is the fluid density, g

is the gravitational acceleration and Re is the particle Reynolds number with $Re = D \cdot w_s \cdot \rho_w / \mu$.

The floc density ρ_{Fi} can be expressed by:

$$\rho_{Fi} = \rho_w + (\rho_p - \rho_w) \cdot \left(\frac{D_p}{D_{Fi}}\right)^{3-n_f} \quad (12)$$

The erosion and deposition are following the empirical Partheniades-Krone formula (Winterwerp and van Kesteren, 2004). Different from that given in Lee et al. (2014) that only allows microflocs to be eroded, this study assumes the eroded sediments assigned to each size groups based on their mass fraction. It is critical to note that in fact the critical shear stress of each size class should be different, since small flocs are easier to resuspend while large flocs may be destroyed due to high shear at the bottom. This part can be improved after the physical process is better understood.

3.2 Hydrodynamics and model setup

The hydrodynamic model is based on the TELEMAC-3D model (www.opentelemac.org) which was developed by the LNHE (Laboratoire National d'Hydraulique et Environnement) of EDF (Electricité De France). It is a finite element solver for the use in free-surface flow for many applications (e.g., Bi and Toorman, 2015; Pu et al., 2016; Davies and Robins, 2017). It solves the Saint-Venant equations for the varying water depth and current velocities. A simple parabolic eddy viscosity profile is assumed to be suitable in this well-mixed area (Shen et al., 2018). The five parameters in Section 3.1, i.e., N_P , N_{F1} , N_{F2} , N_{T1} and N_{T2} , are defined as passive tracers in TELEMAC as long as flocculation is toggled on. The mesh is composed of triangular prisms, with the horizontal two-dimensional mesh created using BlueKenue and with evenly spaced planes (i.e., sigma grid) along the vertical. For the lateral liquid boundary conditions up and downstream in the 1DV application, the discharge is set to zero to disregard advection terms. A

hydraulic rough regime is assumed at the bottom with a friction coefficient of 65 using Chézy's law (Bi, 2015). Also, a single homogeneous sediment bed layer is assumed with infinite thickness, e.g., set as 10 m (Ernst, 2016). The flocculation module can be triggered by an additional key word defined in TELEMAC dictionary file 'telemac3d.dico'. The main subroutine *telemac3d.f* and other subroutines relating to the variable or function declaration, tracer source and sink terms, boundary conditions, turbulence scheme and settling velocity calculations should be modified as well. Detailed information on the corresponding modified subroutines can be found in Shen et al. (2018).

4. Results and discussion

4.1 Biomass-affected SPM dynamics

Focusing on the biomass-affected day with maximum Chl *a* concentration (May 8th, 2013), we choose two complete Tidal Cycles (TCs) starting from the low water and ending at the second further. The mean water depth was 10.5 m during that period with a tidal range of 4 m (Fig. 5a). The maximum along-shore currents during flood are slightly (~ 1 hr) before high water, and the maximum ebb occurs around low water, while cross shore currents are always small (Fig. 5c). The shear velocity u^* has its local maximum at maximum flood or ebb and its local minimum at slack tides. Since flood currents (~ 0.75 m/s) are stronger than ebb currents (~ 0.55 m/s) at 2 mab, the local maximum of u^* at flood (~ 4.5 cm/s) are larger than that at ebb (~ 3.5 cm/s) (Fig. 5b). The significant wave height H_s was less than 0.4 m during most of the time (Fig. 5d), which indicates that the forcing of wind and waves can be neglected during this period. As shown in Figs. 5e to 5g, the median size D_{50} is large (~ 140 μm), the optical transmission is high (~ 0.8) and the TVC measured by the LISST is low (~ 0.15 mL/L) around slack tide; in contrast,

when it is close to the maximum flood/ebb, there are local minima for D_{50} (50 – 80 μm) and optical transmission (0.25 – 0.45) while a local maximum for TVC (> 1.5 mL/L) occurs. This is because the low turbulence around slack tide makes sediment easier to flocculate and to settle down, which results in larger flocs, lower SPM concentration and more sediment concentrated on the bed. The SPM concentrations from OBSs generally follow the trend of TVC, with the SPM at 0.2 mab and 2 mab close to each other except during flood tide (Fig. 5h). Notice that there is another phase-lag between the current velocities and the sediment concentrations in a way that the SPM concentration lags behind the current velocities (Figs. 5c and 5h). This is because it requires time for the flocs to settle out during decreasing flows or to be transported from high concentration areas to low concentration areas (Yu et al., 2011). Focusing on TC2 in Fig. 5a, the hourly FSD plots show obvious multi-modal FSDs appeared around the maximum flood while a unimodal FSD occurred during other times (Fig. 6). This may be because the strong flood has transported large flocs from other locations that result in the observed FSDs skewed toward the megaflocs.

4.2 Biomass-affected FSDs in numerical simulations

The flocculation model described in Section 3 is adopted to better examine the variations of sizes and mass fractions of floc subpopulations. By trial-and-error, the best quality simulation was achieved by selecting collision efficiency $\alpha = 0.2$ and breakage fitting parameter $E_b = 1.0 \times 10^{-4}$. It assumes that when a parent macrofloc/megafloc breaks up, 20% of its mass will release elementary microflocs ($f_{P1} = f_{P2} = 0.2$). The rest 80% mass of the parent megafloc, when destroyed, generates two daughter macroflocs (i.e., $K_2 = 2$); in the case of the parent macrofloc splitting up, the rest 80% mass creates an average number of 1.5 daughter macroflocs (i.e., $K_1 =$

1.5). The selection of K_1 confirms the conclusion by Shen et al. (2018) that this value is a statistical parameter and may not be an integer in the field. Actually $K_1 = 1.5$ means the breakage of a large macrofloc will result in 50% possibility to form one small macrofloc and 50% possibility to form two small macroflocs, together with a few microflocs. The coefficient γ_F in computing the microfloc carrying capacity K (Eq. 9), which considers the size increase because of biofilm bridging, is set as 0.45. This parameter controls the maximum possible size of microflocs, since the growth of a floc cannot be infinitely continued. The floc biomass growth rate r_B is selected as $2.0 \times 10^{-5}/s$ in this study, which is one order of magnitude smaller than the value given by Maggi (2009) in the site Zeebrugge for microbe growth. The initial SPM concentration is set as 0.2 g/L and is uniformly distributed in the water column. The initial size of microflocs, macroflocs and megaflocs, are selected as 12 μm , 100 μm and 300 μm , with their mass percentage 10%, 10% and 80% respectively, based on observations. The time variation of water depth H and shear velocity u^* (Figs. 5a and 5b) are imposed in TELEMAC-3D as the model inputs (Lee et al., 2014; Shen et al., 2018). It is also noted that the starting moment of the model is not Julian day 127.6 as shown in Fig. 5. In fact, the model is started one day before to allow flocs to grow to a quasi-equilibrium state. The critical shear stress for erosion is selected as 1.0 Pa and the empirical erosion parameter is $1.0 \times 10^{-4} \text{ kg}\cdot\text{m}^{-2}\cdot\text{s}^{-1}$. The floc characteristic parameters of microfloc density ρ_P and average fractal dimension nf are set to 2200 kg/m^3 and 2.3 respectively. These parameters are chosen either based on measurements or previous studies. A summary of the main parameters in the simulation was summarized in Table 2.

The simulated floc sizes and settling velocities are weighted based on the mass fraction of each size groups. Thus, the predictions of the weighted mean floc size D_M , the weighted settling velocity w_s and the FSDs (i.e., the floc sizes and their mass fractions of microflocs, macroflocs

and megaflocs) show a reasonable match with the measurements (Fig. 7). Model results show that the size of microflocs D_P nearly double (mean: 21 μm) because of biofilm growth, with small fluctuations (standard deviation: 1.6 μm) responding to different shear rates. During the peak ebb (close to low water in Fig. 7a), the mean size D_M and settling velocity w_s reach their local minimum around 50 μm and 0.5 mm/s (Figs. 7b and 7c). Both of the representative sizes of macroflocs and megaflocs decrease with sizes around 50 μm and 200 μm (Fig. 7d) and their mass fractions around 65% and 5% respectively. The mass fraction of microflocs is around 30% (Figs. 7e). This is because strong peak flows destroy the large and weak flocs, which result in the creation of more compact microflocs. During the slack flow, however, D_M and w_s reach their local maximum. In addition, both of the representative sizes of macroflocs and megaflocs increase with sizes around 120 μm and 320 μm , whereas their mass fractions are almost unchanged for macroflocs and increased for megaflocs ($\sim 20\%$) respectively. The mass fraction of microflocs is reduced to less than 20%. This demonstrates that the flocculation is promoted to generate more large flocs. Although our predictions are in general reasonable, some deviations appear during peak flood period until the time before high slack, which results in a Mean Average Error (MAE) of 16 μm for measured and predicted D_M . The mass fraction of microflocs is overestimated during this period, which leads to an underestimation of the mean size D_M . This may be because in this case the relatively high shear rates during flood flow do not intensively tear large megaflocs. Therefore, the number of microflocs is not significantly increased. This part can be improved with a more detailed investigation of the local hydrodynamics, if ADCP measurements are available in this station in later years. The MAE for mass fraction of microflocs is 0.04, the same as the MAE for mass fraction of microflocs & macroflocs. The MAEs of sizes of megaflocs (D_{F2}) are larger than macroflocs (D_{F1}), with their MAEs 74 μm (\sim

25 %) and $17 \mu\text{m}$ ($\sim 19 \%$) respectively, indicating a lower accuracy of predicted megaflocs. In addition, it is interesting to notice that our prediction of w_s is smaller than the value based on the method by Markussen and Andersen (2013) (MAE: 0.24 mm/s), but represents a better match with Lee et al. (2012) (MAE: 0.22 mm/s).

For TC2, the profiles of eddy viscosities, local SPM concentration, mean size and FSDs are represented every 3 hrs and are compared with observations if available (Fig. 8a). The eddy viscosity ν_t provides the flow turbulence that can enhance or reduce flocculation. The ν_t profiles are bell-shaped with the maximum values in the middle (Fig. 8b). The maximum eddy viscosities are around $0.04 \text{ m}^2/\text{s}$ and $0.01 \text{ m}^2/\text{s}$ at peak flows and slack tides respectively. The profiles of local SPM concentration also vary over time in the tidal cycle (Fig. 8c), neglecting the particles transported from other sites. High turbulence during maximum flood or ebb makes the sediment better well-mixed than the period close to slack tide. This is because large flocs appear during slack because of low turbulence and large differential settling, and thus are easier to settle to the bed. Note that the possible stratification due to sediment concentration, which may result in the ν_t profiles skewing towards the bed, is not included in the present model. This part can be enhanced when the erosion and deposition of bed sediments are better addressed. The predicted mean size D_M decreases from top to the bottom, with the value at 2 mab reasonably agrees with observations (Fig. 8d). This suggests that more large aggregates appear at the surface probably because of low turbulence and sufficient sunlight for the growth of biomineral flocs, and more small particles close to the bottom because of high shear rates. The predicted trend of D_M is similar to other studies that are also focusing on the Belgian coastal area (Lee et al., 2014). At 2 mab, the simulated and measured FSDs also show a suitable match (Fig. 8e). Better predictions are achieved at $t = 0$ and $t = 12$ hr. At $t = 6$ hr, the fraction of microflocs are overestimated which

lead to a smaller value of predicted D_M (Fig. 8d). This may be because the turbulence is not as strong as expected to break up more flocs. At $t = 3$ hr and $t = 9$ hr, the simulated number of megaflocs is larger than observation. This may be because biological activity is higher when the fluid velocity is low, which leads to the abundance of megaflocs during the algae bloom period.

4.3 Role of biomass in flocculation

In order to investigate the effect of bioactivity on flocculation during the peak algae bloom period, the model also predicts the mean size D_M and settling velocity w_s without biofilm growth, by setting the specific growth rate r_B equal to null (Fig. 9). Based on our simulations, the mean sizes D_M decrease by 25% during peak flow if biological effects are neglected (Fig. 9a). During slack tides, however, the predicted weighted mean sizes D_M under biomass-affected and biomass-free conditions are close (with a maximum of 10% difference). The MAE of D_M almost doubles (from 16 μm to 29 μm) when biological effects are ignored. On the other hand, the predicted settling velocities w_s are always much higher with biological effect than without it (Fig. 9b). At peak flow, the biomass-affected w_s are 0.5 mm/s and 0.7 mm/s for maximum flood and ebb respectively, whereas the w_s under biomass-free conditions are 0.2 mm/s for both. Similarly, the w_s decreases from 1.2 mm/s to 0.6 mm/s at low slack, and from more than 1.5 mm/s to less than 1 mm/s at high slack. Without biomass effects, the MAE of w_s has increased to 0.32 mm/s using Lee et al. (2012)'s method. The relationships of D_M and w_s show that during peak flows, larger mean floc sizes, although with reduced floc densities, result in higher settling velocities when biofilm growth are considered. However, during slack flows, it shows that a comparable mean size D_M coincides with a higher settling velocity with biological effects. This is because when biomass is absent, the mass fraction of megaflocs is overestimated while their

representative size D_{F2} (and thus the macrofloc settling velocity $w_{s,F2}$) is underestimated, with the net effect of comparable D_M and smaller mean w_s . Only by considering the floc growth due to organism colonization can the megaflocs further be enlarged to achieve better predictions.

A biomass-poor period on October 8th (Julian day 280) in the year 2013 is investigated to compare with biomass-rich period on May 8th (Fig. 10). The mean depth is 10.7 m and the tidal range 4.5 m (spring tide). Peak SPM concentrations at 0.2 mab and 2 mab are around 0.4 g/L and 0.8 g/L, more than double compared with the algae bloom period. The cross-shore current is dominant, with peak flow 0.8 m/s at both maximum flood and maximum ebb. The significant wave is small and can be neglected as well. Again, the time variations of water depth and shear velocity are the model inputs, while Figs. 10e to 10h are model predictions. The initial fractions of microflocs, macroflocs and megaflocs are set as 10%, 80% and 10% respectively. The mass fractions of created microflocs when a macrofloc or megafloc breaking up are slightly changed, and set as $f_{P1} = 0.3$ and $f_{P2} = 0.1$. Other parameters are the same as in the previous case with the biofilm growth term deactivated. It shows that the predicted mean size D_M , mean settling velocities w_s and FSDs in general agree well with measurements. The MAEs of observed and simulated sizes of macroflocs and megaflocs are 22 μm ($\sim 29\%$) and 101 μm ($\sim 33\%$) respectively, with the MAE of w_s 0.21 mm/s ($\sim 29\%$ using Lee et al. (2012)'s method). The largest deviation between simulation and observations also occurs when currents vary from peak flood to high slack. It is interesting to notice that, different from the algae bloom period, the predictions of D_M and w_s are higher than the measurements (Figs. 10e and 10f). This is because the modeled mass fractions of megaflocs are higher than observations while the simulated mass fractions of microflocs are lower (Fig. 10f). At this time, perhaps the turbulence is higher than expected, allowing to split large and weak megaflocs when they cannot withstand the strong

shear. The MAE of mass fractions of microflocs is 0.08 and the MAE of mass fractions of microflocs & macroflocs is 0.09. The D_M and w_s (by Lee et al. (2012)'s method) in biomass-rich periods (mean: 90 μm and 1 mm/s) is higher than that in biomass-poor periods (mean: 81 μm and 0.72 mm/s), which indicates an enhanced flocculation due to bioactivities in early May. Specifically, the sizes of megaflocs only represent small variations between biomass-rich (mean: 300 μm) and biomass-poor (mean: 305 μm) periods, with their mean mass fractions also close. The sizes of macroflocs show relatively larger differences: mean value of 90 μm during biomass-rich periods vs. 75 μm during biomass-poor periods. The macroflocs are more abundant in biomass-rich May (mean: 69 %) than in biomass-poor October (mean: 60 %), and the case is opposite for microflocs (22 % in May and 32 % in October).

4.4 Implications

The occurrence of SPM generated by natural processes or by the impact of human activities is of great interest to scientists and engineers. By flocculation, smaller particles aggregate into larger ones and change thus the settling velocities and downward flux of the SPM. Large amount of money are spend each year on dredging and dumping activities necessary to keep navigation channels and harbors accessible, on the treatment of contaminated dredged sediments, on the recovery of reservoir capacity and fisheries habitat, and on drinking water and wastewater treatments (Droppo et al., 2005). Nevertheless, only recently has the biological flocculation of cohesive sediments been highlighted as a significant mechanism in natural systems, since the microbes colonizing the attached biomass significantly modify the SPM properties. The microbial activities highly relate to their ambient environments (such as turbulence, nutrients, temperature, PH and UV exposure), which may be described by advanced

(such as reviewed by Lai et al., 2018) but efficient microbial models to account for the processes of prey, metabolism, decay, ions bridging and mineralization. The Belgian coast is a typical area with high primary production during algae bloom periods and low ones during fall and winter. The relatively less complicated hydrodynamics in Belgian coastal area (i.e., well-mixed in general) enable researchers to focus on the aggregation and breakage processes, which make this region a “field laboratory” to test hypothesis from laboratory studies. The findings and the simplified models validated in this area can be extended to other non-stratified regions such as the Delaware Bay, and can serve as a first indication of more complicated (partially) stratified regions such as the Chesapeake Bay and the Yangtze River Estuary. The model may also be extended to reproduce the seasonal (from spring to winter) and spatial (from nearshore to offshore) variations of FSDs with a better understanding of the roles of biomass in flocculation processes of biomineral flocs.

5. Conclusions

The bio-mediated flocculation and SPM dynamics were examined with a case study from the Belgian coastal zone. Data were collected at station MOW1 near the harbor of Zeebrugge during periods with peak and low Chl *a* concentration in the year 2013. All the observed flocs are classified into microflocs, macroflocs and megaflocs; therefore, the FSDs are represented by the sizes and mass fractions of the above three size classes. We have observed that the flocculation is enhanced during high-biomass periods due to the occurrence of biological glue and organic particle that are attached to the mineral particles in suspension to form biomineral flocs. During the two contrasting periods that represent the seasonal patterns, the results indicate that the mean sizes of megaflocs are close, while the mean sizes of macroflocs are larger in

biomass-rich May than in biomass-poor October. Within a tidal cycle, the settling velocities are high at slack tides when turbulence is reduced but low at low and high tides. In addition, a new flocculation model was developed under the population balance framework, assuming larger macroflocs or megaflocs composed of elementary microflocs. The flocculation processes are clarified based on six aggregation, two breakage and one biofilm growth processes. The aggregation processes include a two-body collision between flocs in the same or different classes. The breakage processes describe the destruction of macroflocs or megaflocs resulting in the release of some constituted microflocs and one or two daughter macroflocs. It is noticed that flocs also grow because of biofilm attachment with EPS bridging. Therefore, the growth of any floc due to biological activities is averaged to the biofilm growth of the elementary microflocs. The specific maximum growth rate r_B and the carrying capacity of microflocs K are the two key parameters to determine the biological effects. This simple bio-flocculation model was successfully coupled in the open TELEMAC-3D model with five passive tracers: the number density of microflocs, macroflocs and megaflocs in suspension (N_P , N_{F1} and N_{F2}), and the total number of microflocs in macroflocs (N_{T1}) or megaflocs (N_{T2}). When the growth term was removed, the model simulations show a clear underestimation of the floc settling velocities. This model also reasonably predicted the FSDs at biomass-poor period without the biomass growth term. With better understanding of other key processes such as the erosion and deposition criteria for different size classes, model performance will be enhanced to better predict and explain the dynamics of estuarine particles.

Acronyms

ADCP Acoustic Doppler Current Profiler

ADV	Acoustic Doppler Velocimeter
EPS	Extracellular Polymeric Substance
FSD	Floc Size Distribution
LISST	Laser In Situ Scattering and Transmissometry
MAE	Mean Absolute Error
OBS	Optical Backscatter Sensor
POC	Particulate Organic Carbon
PON	Particulate Organic Nitrogen
SPM	Suspended Particulate Matter
TC	Tidal Cycle
TEP	Transparent Exopolymer Particle
TVC	Total Volume Concentration

Acknowledgements

The authors would like to acknowledge the financial support from the BRAIN.be project INDI67 and the JPI Oceans Microplastics project WEATHER-MIC, both funded by the Belgian Science Policy Office (BELSPO). Additional support is provided by the Open Research Fund of State Key Laboratory of Estuarine and Coastal Research (Grant number: SKLEC-KF201811). We would also like to thank the three anonymous reviewers who helped to improve this manuscript.

References

- Adriaens, R., Zeelmaekers, E., Fettweis, M., Vanlierde, E., Vanlede, J., Stassen, P., Elsen, J., Srodon, J., Vandenberghe, N., 2018. Quantitative clay mineralogy as provenance indicator for recent muds in the southern North Sea. *Marine Geology* 398, 48–58.
- Allredge, A.L., Passow, U., Logan, B.E., 1993. The abundance and significance of a class of large, transparent organic particles in the ocean. *Deep-Sea Research Part I - Oceanographic Research Papers* 40(6), 1131–1140.
- Andersen, T.J., Pejrup, M., 2011. Biological influences on sediment behavior and transport. *In*: McLusky, D., Wolanski, E. (Eds.), *Treatise on Estuarine and Coastal Science*, Waltham, Academic Press, pp. 289–309.
- Arndt, S., Lacroix, G., Gypens, N., Regnier, P., Lancelot, C., 2011. Nutrient dynamics and phytoplankton development along an estuary–coastal zone continuum: A model study. *Journal of Marine Systems* 84, 49–66.
- Baeye, M., Fettweis, M., Voulgaris, G., Van Lancker, V., 2011. Sediment mobility in response to tidal and wind-driven flows along the Belgian inner shelf, southern North Sea. *Ocean Dynamics* 61, 611–622.
- Bar-Zeev, E., Passow, U., Castrillon, S.R.V., Elimelech, M., 2015. Transparent exopolymer particles: From aquatic environments and engineered systems to membrane biofouling. *Environmental Science & Technology* 49, 691–707.
- Bhaskar, P.V., Bhosle, N.B., 2005. Microbial extracellular polymeric substances in marine biogeochemical processes. *Current Science* 88, 45–53.

- Bi, Q., 2015. Numerical modelling of near-bottom sediment transport: Turbulence modulation, new process models and application to the Scheldt & the Belgian coast. (Ph.D. dissertation) KU Leuven, Belgium.
- Bi, Q.L., Toorman, E.A., 2015. Mixed-sediment transport modelling in Scheldt estuary with a physics-based bottom friction law. *Ocean Dynamics* 65, 555–587.
- Camp, T.R., Stein, P.C., 1943. Velocity gradients and internal work in fluid motion. *Journal of the Boston Society of Civil Engineers* 30, 219–237.
- Capuzzo, E., Stephens, D., Silva, T., Barry, J., Forster, R. M., 2015. Decrease in water clarity of the southern and central North Sea during the 20th century. *Global Change Biology* 21, 2206–2214.
- Cartwright, G.M., 2013. Application of acoustics and optics for the characterization of suspended particulate matter within an estuarine observing system. (Ph.D. Dissertation) Virginia Institute of Marine Science, The College of William and Mary, Gloucester Point, Virginia, USA.
- Chen, P., Yu, J.C.S., Fettweis, M., 2018. Modeling storm-influenced suspended particulate matter flocculation using a tide–wave–combined biomineral model. *Water Environment Research* 90, 244–257.
- Chen, X.D., Zhang, C.K., Zhou, Z., Gong, Z., Zhou, J.J., Tao, J.F., Paterson, D.M., Feng, Q., 2017. Stabilizing effects of bacterial biofilms: EPS penetration and redistribution of bed stability down the sediment profile. *Journal of Geophysical Research: Biogeosciences* 122, 3113–3125.
- Davies, A.G., Robins, P.E., 2017. Residual flow, bedforms and sediment transport in a tidal channel modelled with variable bed roughness. *Geomorphology* 295, 855–872.

De Jonge, V.N., Schuttelaars, H.M., Van Beusekom, J.E.E., Talke, S.A., De Swart, H.E., 2014.

The influence of channel deepening on estuarine turbidity levels and dynamics, as exemplified by the Ems estuary. *Estuarine, Coastal and Shelf Science* 139, 46–59.

Demirak, A., Yilmaz, H.A., Keskin, F., Sahin, Y., Akpolat, O., 2012. Investigation of heavy metal content in the suspended particulate matter and sediments of inner Gokova Bay and creeks. *Environmental Monitoring and Assessment* 184, 7113–7124.

Discart, V., 2015. Transparent exopolymer particles: detection and role in membrane based systems. (Ph.D. Dissertation) KU Leuven, Belgium.

Droppo, I.G., 2001. Rethinking what constitutes suspended sediment. *Hydrological Processes* 15, 1551–1564.

Droppo, I.G., Leppard, G.G., Flannigan, D.T., Liss, S.N., 1997. The fresh water floc: A functional relationship of water and organic and inorganic floc constituents affecting suspended sediment properties. *Water Air and Soil Pollution* 99, 43–53.

Droppo, I.G., Leppard, G.G., Liss, S.N., Milligan, T.G., 2005. Flocculation in natural and engineered environmental systems. CRC Press, Florida, USA.

Edelvang, K., Austen, I., 1997. The temporal variation of flocs and fecal pellets in a tidal channel. *Estuarine, Coastal and Shelf Science* 44, 361–367.

Eisma, D., 1991. Particle size of suspended matter in estuaries. *Geo-Marine Letters* 11, 147–153.

Ernst, S., 2016. Implementation of a flocculation model in TELEMAC-3D. (Master's thesis) KU Leuven, Belgium.

Fang, H.W., Lai, H.J., Cheng, W., Huang, L., He, G.J., 2017. Modeling sediment transport with an integrated view of the biofilm effects. *Water Resources Research* 53, 7536–7557.

- Fettweis, M., Francken, F., Pison, V., Van den Eynde, D., 2006. Suspended particulate matter dynamics and aggregate sizes in a high turbidity area. *Marine Geology* 235, 63–74.
- Fettweis, M., Francken, F., Van den Eynde, D., Verwaest, T., Janssens, J., Van Lancker, V., 2010. Storm influence on SPM concentrations in a coastal turbidity maximum area with high anthropogenic impact (southern North Sea). *Continental Shelf Research* 30, 1417–1427.
- Fettweis, M., Baeye, M., Van der Zande, D., Van den Eynde, D., Lee, B.J., 2014. Seasonality of floc strength in the southern North Sea. *Journal of Geophysical Research: Oceans* 119, 1911–1926.
- Fettweis, M., Baeye, M., 2015. Seasonal variation in concentration, size, and settling velocity of muddy marine flocs in the benthic boundary layer. *Journal of Geophysical Research: Oceans* 120, 5648–5667.
- Fettweis, M., Baeye, M., Cardoso, C., Dujardin, A., Lauwaert, B., Van den Eynde, D., Van Hoestenbergh, T., Vanlede, J., Van Poucke, L., Velez, C., Martens, C., 2016. The impact of disposal of fine-grained sediments from maintenance dredging works on SPM concentration and fluid mud in and outside the harbor of Zeebrugge. *Ocean Dynamics* 66, 1497–1516.
- Fettweis, M., Lee, B.J., 2017. Spatial and seasonal variation of biomineral suspended particulate matter properties in high-turbid nearshore and low-turbid offshore zones. *Water* 9, 694.
- Fugate, D.C., Friedrichs, C.T., 2002. Controls on suspended aggregate size in partially mixed estuaries. *Estuarine, Coastal and Shelf Science* 58, 389–404.
- Guo, C., He, Q., Guo, L., Winterwerp, J.C., 2017. A study of in-situ sediment flocculation in the turbidity maxima of the Yangtze Estuary. *Estuarine, Coastal and Shelf Science* 191, 1–9.
- Ittekkot, V., 1988. Global trends in the nature of organic matter in river suspensions. *Nature* 332, 436–438.

- Jackson, G.A., 1990. A model of the formation of marine algal flocs by physical coagulation processes. *Deep-Sea Research Part A - Oceanographic Research Papers* 37, 1197–1211.
- Jackson, G.A., Burd, A.B., 2015. Simulating aggregate dynamics in ocean biogeochemical models. *Progress in Oceanography* 133, 55–65.
- Keil, R. G., Montluçon, D. B., Prahl, F. G., Hedges, J. I., 1994. Sorptive preservation of labile organic matter in marine sediments. *Nature* 370, 549–552.
- Keyvani, A., Strom, K., 2014. Influence of cycles of high and low turbulent shear on the growth rate and equilibrium size of mud flocs. *Marine Geology* 354, 1–14.
- Kitheka, J.U., Mavuti, K.M., Nthenge, P., Obiero, M., 2016. The turbidity maximum zone in a shallow, well-flushed Sabaki estuary in Kenya. *Journal of Sea Research* 110, 17–28.
- Lee, B.J., Toorman, E., Molz, F.J., Wang, J., 2011. A two-class population balance equation yielding bimodal flocculation of marine or estuarine sediments. *Water Research* 45, 2131–2145.
- Lee, B.J., Fettweis, M., Toorman, E., Molz, F.J., 2012. Multimodality of a particle size distribution of cohesive suspended particulate matters in a coastal zone. *Journal of Geophysical Research - Oceans* 117, C03014.
- Lee, B.J., Toorman, E., Fettweis, M., 2014. Multimodal particle size distributions of fine-grained sediments: mathematical modeling and field investigation. *Ocean Dynamics* 64, 429–441.
- Lee, B.J., Hur, J., Toorman, E.A., 2017. Seasonal variation in flocculation potential of river water: Roles of the organic matter pool. *Water* 9, 335.
- Lai, H., Fang, H., Huang, L., He, G., Reible, D., 2018. A review on sediment bioflocculation: Dynamics, influencing factors and modeling. *Science of The Total Environment* 642, 1184–1200.

- Li, D., Li, Y., Xu, Y., 2017. Observations of distribution and flocculation of suspended particulate matter in the Minjiang River Estuary, China. *Marine Geology* 387, 31–44.
- Lick, W., Huang, H.N., Jepsen, R., 1993. Flocculation of fine-grained sediments due to differential settling. *Journal of Geophysical Research* 98 (C6), 10279–10288.
- Liss, S.N., Droppo, I.G., Flannigan, D.T., Leppard, G.G., 1996. Floc architecture in wastewater and natural riverine systems. *Environmental Science & Technology* 30, 680–686.
- Maerz, J., Hofmeister, R., van der Lee, E.M., Gräwe, U., Riethmüller, R., Wirtz, K.W., 2016. Maximum sinking velocities of suspended particulate matter in a coastal transition zone. *Biogeosciences* 13, 4863–4876.
- Maggi, F., 2005. Flocculation dynamics of cohesive sediment. (Ph.D. Dissertation) Delft University of Technology, Netherlands.
- Maggi, F., Manning, A.J., Winterwerp, J.C., 2006. Image separation and geometric characterisation of mud flocs. *Journal of Hydrology* 326, 325–348.
- Maggi, F., 2007. Variable fractal dimension: a major control for floc structure and flocculation kinematics of suspended cohesive sediment. *Journal of Geophysical Research* 112, C07012.
- Maggi, F., Mietta, F., Winterwerp, J.C., 2007. Effect of variable fractal dimension on the floc size distribution of suspended cohesive sediment. *Journal of Hydrology* 343, 43–55.
- Maggi, F., 2009. Biological flocculation of suspended particles in nutrient-rich aqueous ecosystems. *Journal of Hydrology* 376, 116–125.
- Markussen, T. N., Andersen, T.J., 2013. A simple method for calculating in situ floc settling velocities based on effective density functions. *Marine Geology* 344, 10–18.
- Markussen, T.N., Elberling, B., Winter, C., Andersen, T.J., 2016. Flocculated meltwater particles control Arctic land-sea fluxes of labile iron. *Scientific Reports* 6, 24033.

- Montuori, P., Aurino, S., Garzonio, F., Triassi, M., 2016. Polychlorinated biphenyls and organochlorine pesticides in Tiber River and Estuary: Occurrence, distribution and ecological risk. *Science of the Total Environment* 571, 1001–1016.
- Morelle, J., Schapira, M., Claquin, P., 2017. Dynamics of phytoplankton productivity and exopolysaccharides (EPS and TEP) pools in the Seine Estuary (France, Normandy) over tidal cycles and over two contrasting seasons. *Marine Environmental Research* 131, 162–176.
- Nechad, B., Ruddick, K.G., Park, Y., 2010. Calibration and validation of a generic multisensor algorithm for mapping of total suspended matter in turbid waters. *Remote Sensing of Environment* 114, 854–866.
- Nopens, I., 2005. Modelling the activated sludge flocculation process: a population balance approach. (Ph.D. Dissertation) University of Ghent, Belgium.
- Passow, U., Shipe, R. F., Murray, A., Pak, D. K., Brzezinski, M.A., Alldredge, A.L., 2001. The origin of transparent exopolymer particles (TEP) and their role in the sedimentation of particulate matter. *Continental Shelf Research* 21, 327–346.
- Playter, T., Konhauser, K., Owttrim, G., Hodgson, C., Warchola, T., Mloszewska, A.M., Sutherland, B., Bekker, A., Zonneveld, J.P., Pemberton, S.G., 2017. Microbe-clay interactions as a mechanism for the preservation of organic matter and trace metal biosignatures in black shales. *Chemical Geology* 459, 75–90.
- Pu, X, Shi, J.Z., Hu, G.D., 2016. Analyses of intermittent mixing and stratification within the North Passage of the Changjiang (Yangtze) River estuary, China: A three-dimensional model study. *Journal of Marine Systems* 158, 140–164.

- Redfield, A.C., 1934. On the proportions of organic derivatives in seawater and relation to the composition of the plankton. *In: Daniel, R.J. (Ed) James Johnstone Memorial Volume.* Liverpool University Press, Liverpool, pp 176–192.
- Richardson, J.F., Zaki, W.N., 1954. Sedimentation and fluidisation: Part I. *Transactions of the Institution of Chemical Engineers and the Chemical Engineer* 32, 35–53.
- Riebesell, U., 1991. Particle aggregation during a diatom bloom. II. Biological aspects. *Marine Ecology Progress Series* 69, 281–291.
- Rouhnia, M., Keyvani, A., Strom, K., 2014. Do changes in the size of mudflocs affect the acoustic backscatter values recorded by a Vector ADV? *Continental Shelf Research* 84, 84–92.
- Sahin, C., Guner, H.A.A., Ozturk, M., Sheremet, A., 2017. Floc size variability under strong turbulence: Observations and artificial neural network modeling. *Applied Ocean Research* 68, 130–141.
- Shao, Y.Y., Yan, Y., Maa, J.P.-Y., 2011. In-situ measurements of settling velocity near Baimao Shoal in Changjiang Estuary. *Journal of Hydraulic Engineering* 137, 372–380.
- Shao, Y., Maa, J.P.Y., 2017. Comparisons of different instruments for measuring suspended cohesive sediment concentrations. *Water* 9, 968.
- Shao, Y., Shen, X., Maa, J.P.Y., Shen, J., 2017. Simulating high ebb currents in the North Passage of the Yangtze estuary using a vertical 1-D model. *Estuarine, Coastal and Shelf Science* 196, 399–410.
- Shchepetkina, A., Gingras, M.K., Zonneveld, J.P., Pemberton, S.G., 2017. Silt- and bioclastic-rich flocs and their relationship to sedimentary structures: Modern observations from the Petitcodiac River Estuary. *Estuaries and Coasts* 40, 947–966.

- Shen, X., 2016. Modeling flocculation and deflocculation processes of cohesive sediments. (Ph.D. Dissertation) Virginia Institute of Marine Science, The College of William and Mary, Gloucester Point, Virginia, USA.
- Shen, X., Maa, J.P.Y., 2015. Modeling floc size distribution of suspended cohesive sediments using quadrature method of moments. *Marine Geology* 359, 106–119.
- Shen, X., Maa, J.P.Y., 2016a. A camera and image processing system for floc size distributions of suspended particles. *Marine Geology* 376, 132–146.
- Shen, X., Maa, J.P.Y., 2016b. Numerical simulations of particle size distributions: Comparison with analytical solutions and kaolinite flocculation experiments. *Marine Geology* 379, 84–99.
- Shen, X., Maa, J.P.Y., 2017. Floc size distributions of suspended kaolinite in an advection transport dominated tank: Measurements and modeling. *Ocean Dynamics* 67, 1495–1510.
- Shen, X., Lee, B.J., Fettweis, M., Toorman, E.A., 2018. A tri-modal flocculation model coupled with TELEMAC for estuarine muds both in the laboratory and in the field. *Water Research* 145, 473–486.
- Sherwood, C.R., Lacy, J.R., Voulgaris, G., 2006. Shear velocity estimates on the inner shelf off Grays Harbor, Washington, USA. *Continental Shelf Research* 26, 1995–2018.
- Smith, S.J., Friedrichs, C.T., 2011. Size and settling velocities of cohesive flocs and suspended sediment aggregates in a trailing suction hopper dredge plume. *Continental Shelf Research* 31, S50–S63.
- Smith, S.J., Friedrichs, C.T., 2015. Image processing methods for in situ estimation of cohesive sediment floc size, settling velocity, and density. *Limnology and Oceanography - Methods* 13, 250–264.

- Smoluchowski, M., 1917. Versuch einer Mathematischen Theorie der Koagulationskinetik Kolloider Lösungen. *Zeitschrift für Physikalische Chemie* 92, 129–168. (in German)
- Stanley, C.D., Clarke, R.A., McNeal, B.L., MacLeod, B.W., 2003. Relationship of chlorophyll *a* concentration to seasonal water quality in Lake Manatee, Florida. In: Publication of the Soil and Water Science Department, Florida Cooperative Extension Service, IFAS, University of Florida, EDIS.
- Tang, F.H.M., Alonso-Marroquin, F., Maggi, F., 2014. Stochastic collision and aggregation analysis of kaolinite in water through experiments and the spheropolygon theory. *Water Research* 53, 180–190.
- Tang, F.H.M., Maggi, F., 2016. A mesocosm experiment of suspended particulate matter dynamics in nutrient- and biomass-affected waters. *Water Research* 89, 76–86.
- Tang, F.H.M., 2017. Microbiological modulation of suspended particulate matter dynamics. (Ph.D. Dissertation) The University of Sydney, Australia.
- Thomas, D.G., Judd, S.J., Frawcett, N., 1999. Flocculation modeling: A review. *Water Research* 33, 1579–1592.
- Thornton, D.C.O., 2002. Diatom aggregation in the sea: Mechanisms and ecological implications. *European Journal of Phycology* 37(2), 149–161.
- Tran, D., Strom, K., 2017. Suspended clays and silts: Are they independent or dependent fractions when it comes to settling in a turbulent suspension? *Continental Shelf Research* 138, 81–94.
- Uncles RJ, Stephens JA, Law DJ. 2006. Turbidity maximum in the macrotidal, highly turbid Humber Estuary, UK: Flocs, fluid mud, stationary suspensions and tidal bores. *Estuarine, Coastal and Shelf Science* 67, 30–52.

- Van den Eynde, D., Fettweis, M., 2006. Modelling of fine-grained sediment transport and dredging material dumpings at the Belgian continental shelf. *Journal of Coastal Research* SI 39, 1564–1569.
- Van Leussen, W., 1988. Aggregation of particles, settling velocity of mudflocs: a review. In: Dronkers, J., Van Leussen, W. (Eds.), *Physical Processes in Estuaries*. SpringerVerlag, Berlin, pp. 347–403.
- Van Maren D.S., Winterwerp, J.C., Sas, M., Vanlede, J., 2009. The effect of dock length on harbour siltation. *Continental Shelf Research* 29, 1410–1425.
- Verney, R., Lafite, R., Brun-Cottan, J.C., Le Hir, P., 2011. Behaviour of a floc population during a tidal cycle: laboratory experiments and numerical modelling. *Continental Shelf Research* 31, S64–S83.
- Vincent, C.E., MacDonald, I.T., 2015. A flocculi model for the acoustic scattering from flocs. *Continental Shelf Research* 104, 15–24.
- Winter, C., Becker, M., Ernstsens, V.B., Hebbeln, D., Port, A., Bartholoma, A., Flemming, B., Lunau, M., 2007. In-situ observation of aggregate dynamics in a tidal channel using acoustics, laser diffraction and optics. *Journal of Coastal Research* SI50, 1173–1177.
- Winterwerp, J.C., 1998. A simple model for turbulence induced flocculation of cohesive sediment. *Journal of Hydraulic Research* 36, 309–326.
- Winterwerp, J.C., van Kesteren, W.G.M., 2004. Introduction to the Physics of Cohesive Sediment in the Marine Environment. In: van Loon, T. (Ed.), *WL/ Delft Hydraulics & Delft University of Technology, Delft, The Netherlands*.

- Yu, J.C.S., Chou, T.Y., Yu, H.C., Chen, P., Vanhellemont, Q., Fettweis, M., 2016. Surface suspended particulate matter concentration in the Taiwan Strait during summer and winter monsoons. *Ocean Dynamics* 66, 1517–1527.
- Yu, Q., Flemming, B.W., Gao, S., 2011. Tide-induced vertical suspended sediment concentration profiles: phase lag and amplitude attenuation. *Ocean Dynamics* 61, 403–410.
- Zhang, J.J., Li, X.Y., 2003. Modeling particle-size distribution dynamics in a flocculation system. *AIChE Journal* 49, 1870–1882.
- Zhang, J.F., Zhang, Q.H., 2011. Lattice Boltzmann simulation of the flocculation process of cohesive sediment due to differential settling. *Continental Shelf Research* 31, S94–S105.
- Zhang, J.F., Zhang, Q.H., Maa, J.P.Y., Qiao, G.Q., 2013. Lattice Boltzmann simulation of turbulence-induced flocculation of cohesive sediment. *Ocean Dynamics* 63, 1123–1135.
- Zhang, J.F., Maa, J.P.Y., Zhang, Q.H., Shen, X.T., 2016. Direct numerical simulations of collision efficiency of cohesive sediments. *Estuarine, Coastal and Shelf Science* 178, 92–100.

Figure captions

Fig. 1 Summer (left) and winter (right) averaged near surface SPM concentrations in the Belgian coastal zone (southern North Sea) computed from satellite images covering the period 2003-2011 and using the algorithms of Nechad et al. (2010). The station MOW1 is the place where observation data have been collected for model validation. The x - and y - coordinates are the longitude and latitude.

Fig. 2 Annually chlorophyll-a concentration derived from MODIS satellite at station MOW1 in the year 2013. The dashed line shows chlorophyll-a concentration $3 \mu\text{g/L}$.

Fig. 3 Seasonal variations of POC/SPM ratios and Chl *a* concentration at the station MOW1 derived from in situ water samples. Each point represents the mean and standard deviation of a full tidal cycle measurement. Data have been collected since November 2002 until January 2018 (if data are available) to show the seasonal pattern.

Fig. 4 Schematic diagram for the flocculation of biomineral microflocs, macroflocs and megaflocs. Particles are not drawn to scale.

Fig. 5 Measurements of time variation of (a) water depth H , (b) shear velocity u^* , (c) along-shore and cross-shore current velocities at 2 mab, (d) significant wave H_s , (e) median size D_{50} , (f) LISST optical transmission, (g) total volumetric concentration and (h) SPM concentration at 0.2 and 2 mab during algae bloom period. Data (symbols) in subfigures (b) - (h) are smoothed (solid lines) using MATLAB 'smooth' function to show the trend of the curves.

Fig. 6 Measurements of hourly FSDs for TC2 (as marked in Fig. 5a) by the LISST instrument during the algae bloom period.

Fig. 7 (a) Time variations of water surface η and along-shore current velocity U . (b) - (e) are predictions of (b) mean floc size D_M , (c) mean settling velocity w_s , (d) sizes of macroflocs DF_1 and megaflocs DF_2 and (e) mass fractions of microflocs and microflocs + macroflocs. Lines are

model results and symbols are measurements. The settling velocity given by both Lee et al. (2012) and Markussen and Andersen (2013) are shown in subfigure (c) as references.

Fig. 8 (a) Time variations of surface η and along-shore current velocity U . (b) - (e) are predicted (b) eddy viscosity profiles, (c) local SPM profiles, (d) mean size profiles and (e) the FSDs every 3 hrs within a typical tidal cycle. The grey lines and grey dots in subfigure (d) and (e) are measurements for comparison, and the dark diamonds in subfigure (e) are modeled FSDs.

Fig.9 (a) Time variations of water surface η and along-shore current velocity U . The predicted (b) mean size D_M and (c) mean settling velocity w_s with and without the effect of bio-activities during algae bloom period are shown (lines), compared with measurements (symbols).

Fig. 10 Measurements of (a) water surface η , (b) shear velocity u^* , (c) along-shore and cross-shore current at 2 mab and (d) significant wave H_s , and model predictions of (e) mean sizes D_M , (f) mean settling velocities w_s , (g) sizes of macroflocs and megaflocs and (f) mass fractions of microflocs and microflocs + macroflocs during a biomass-poor period. Notice that symbols are measurements, lines in (a)-(d) are fitted, and lines in (e)-(h) are modeled results.

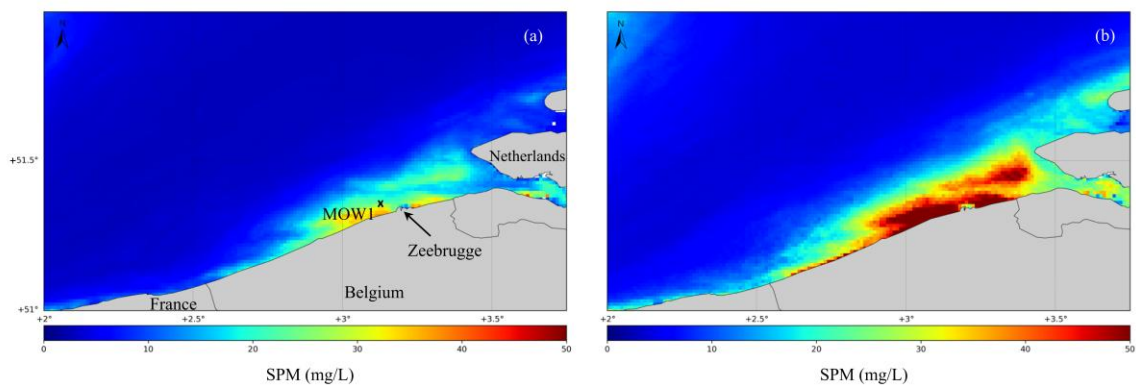


Fig. 1

ACCEPTED

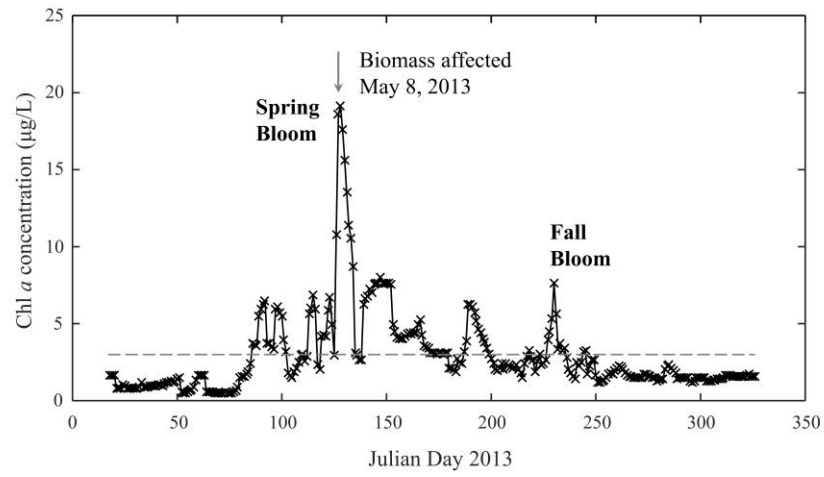


Fig. 2

ACCEPTED

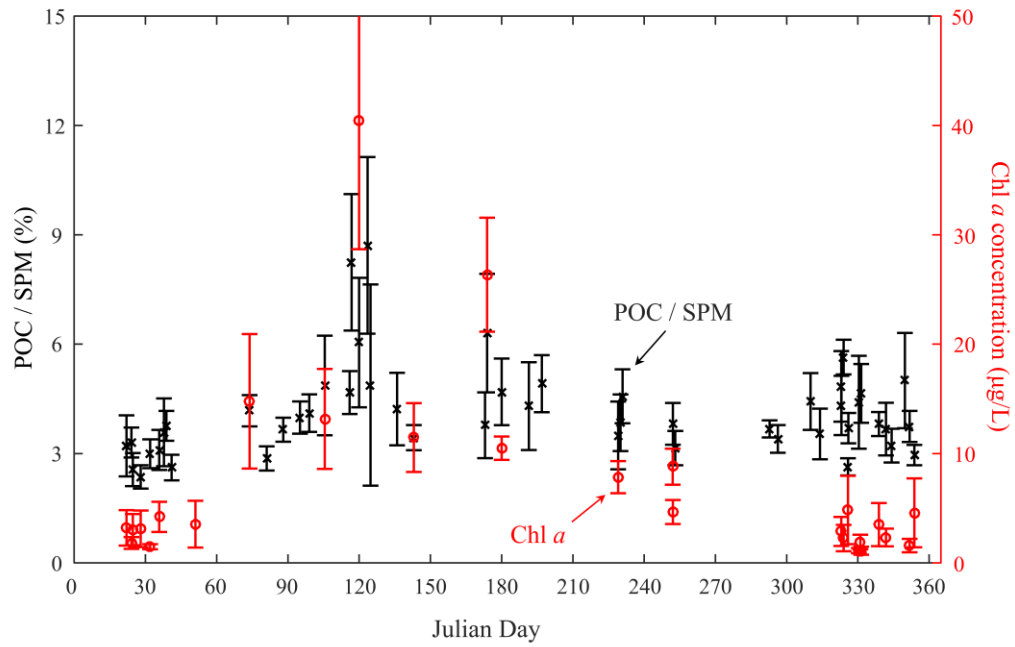


Fig. 3

ACCEPTED

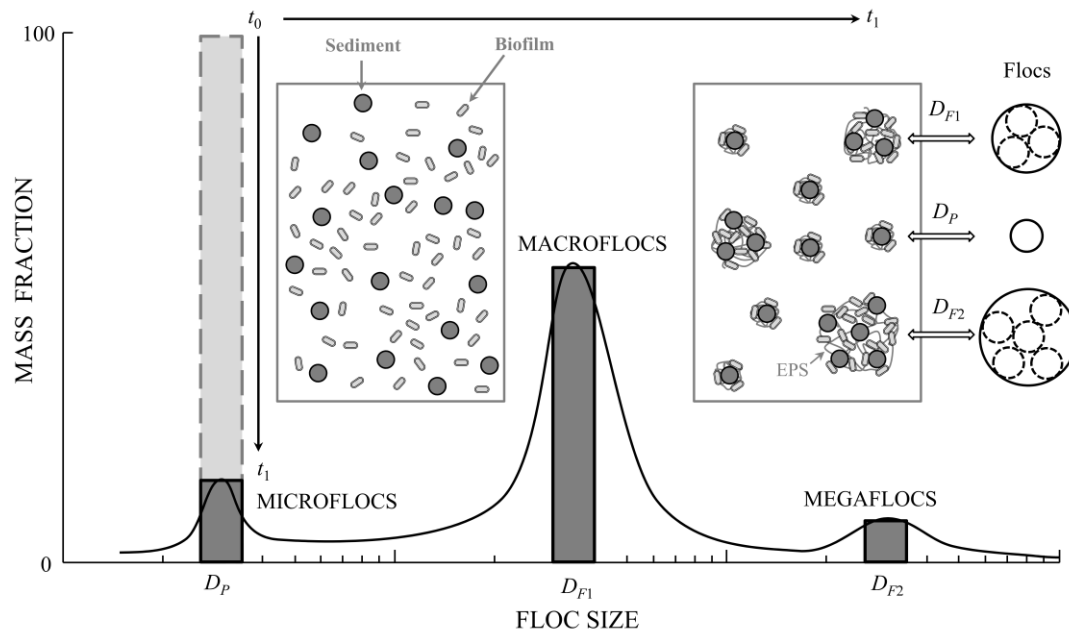


Fig. 4

ACCEPTED

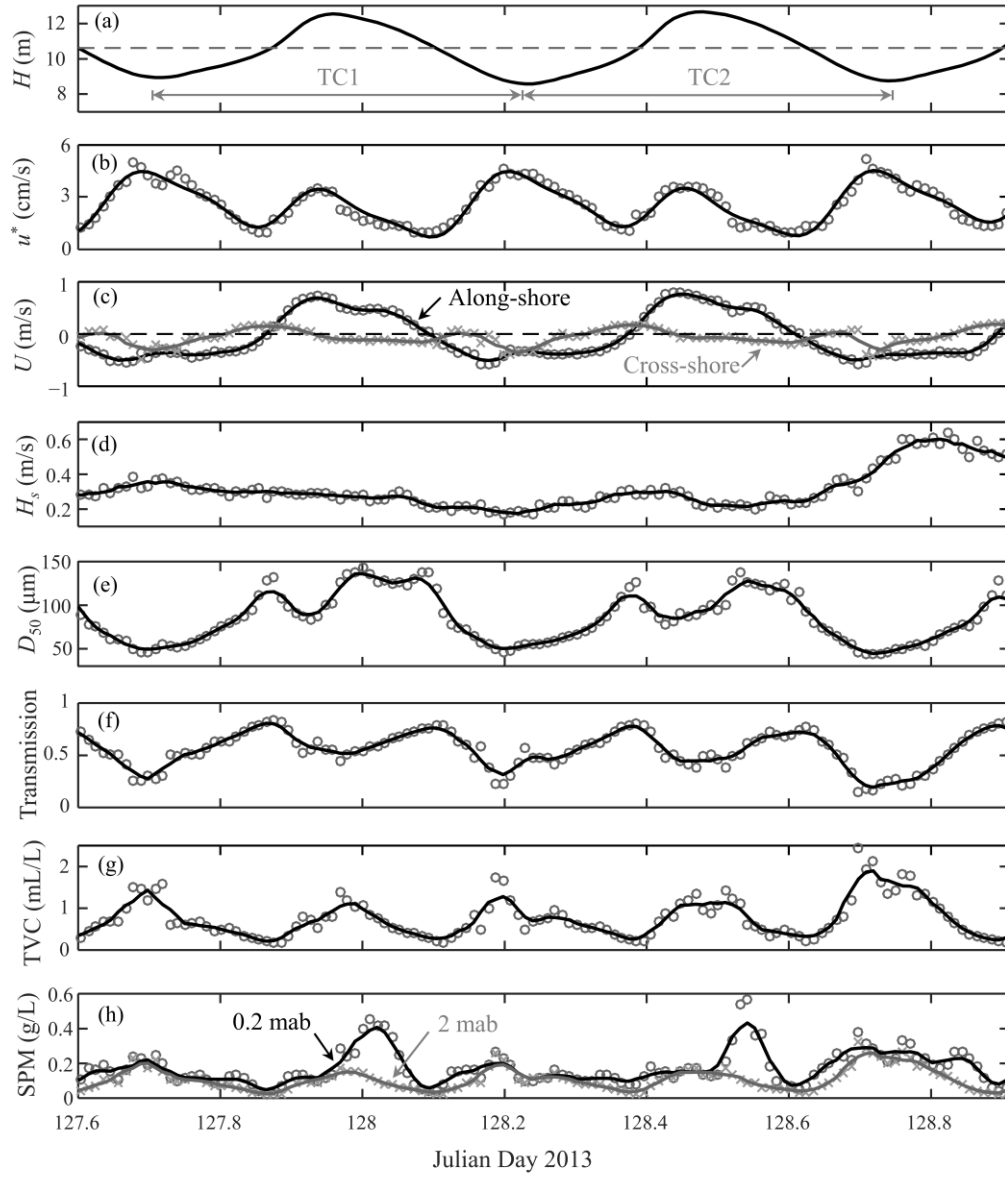


Fig. 5

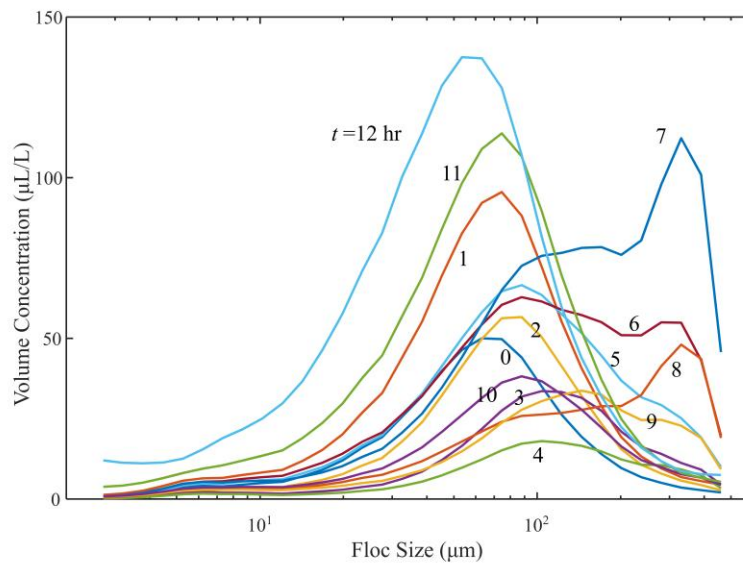


Fig. 6

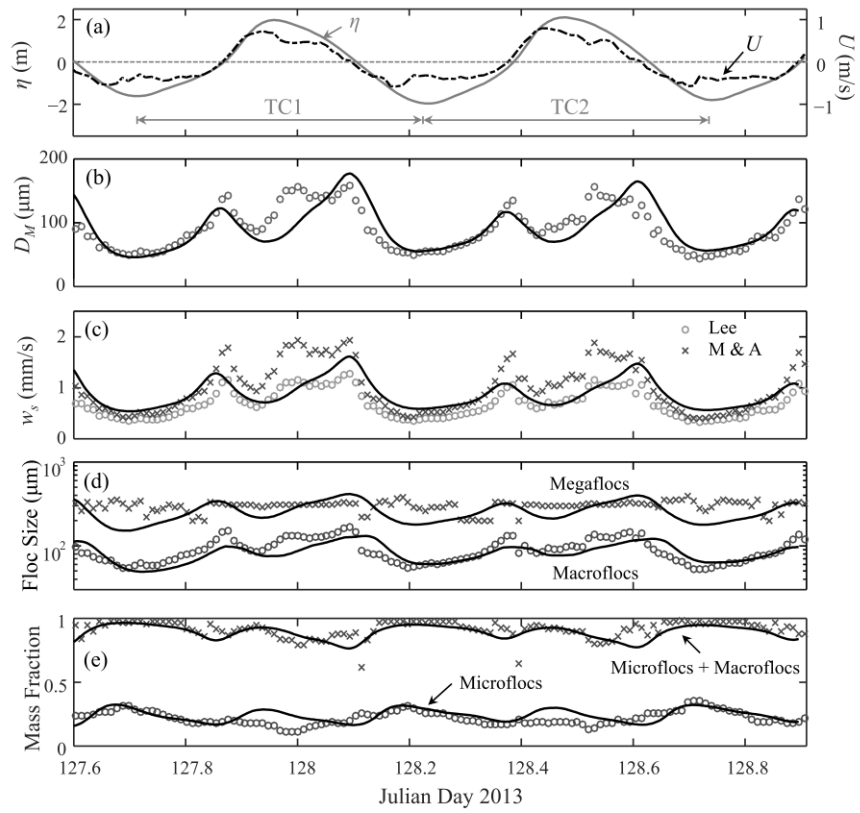


Fig. 7

ACCEPTED

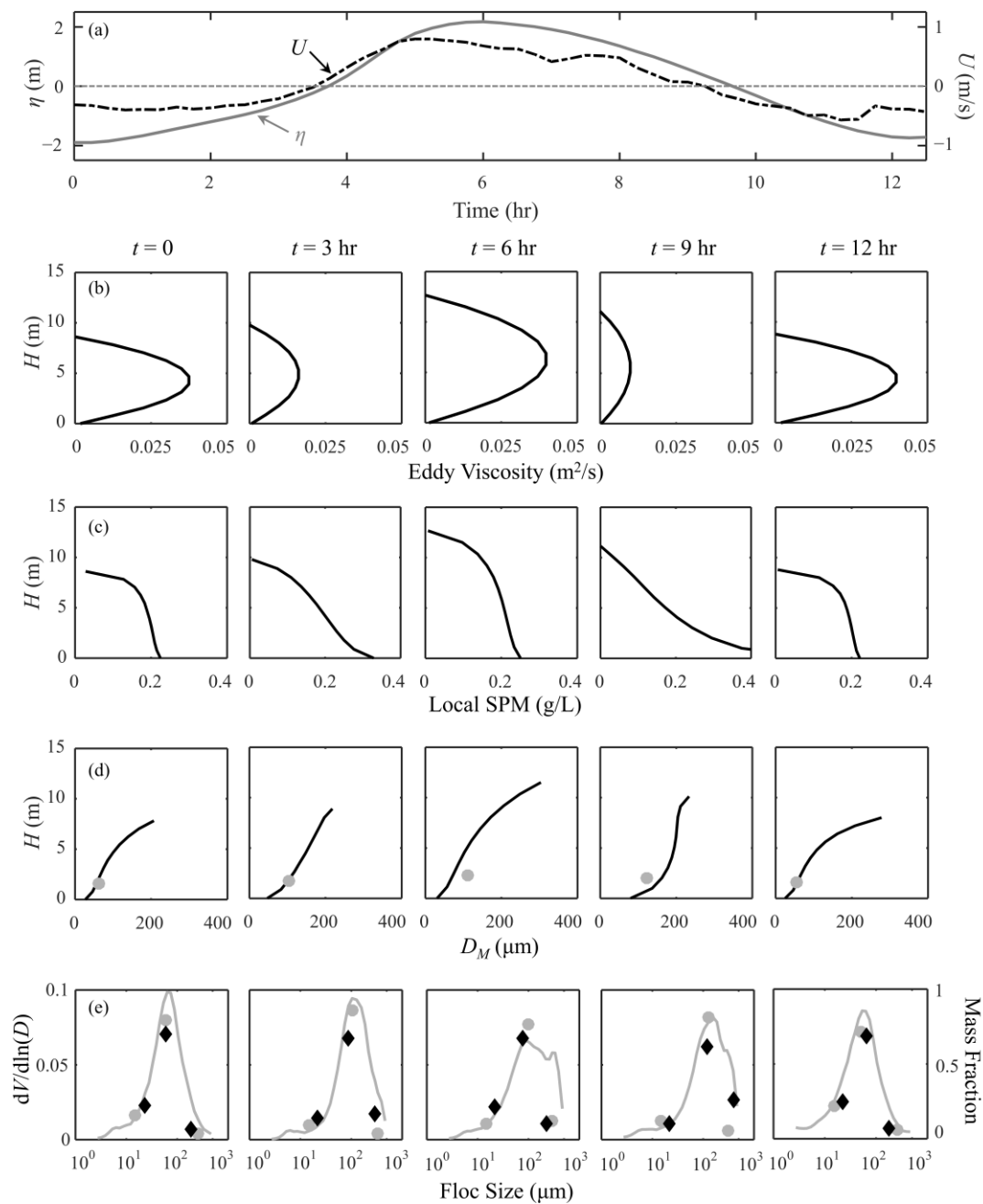


Fig. 8

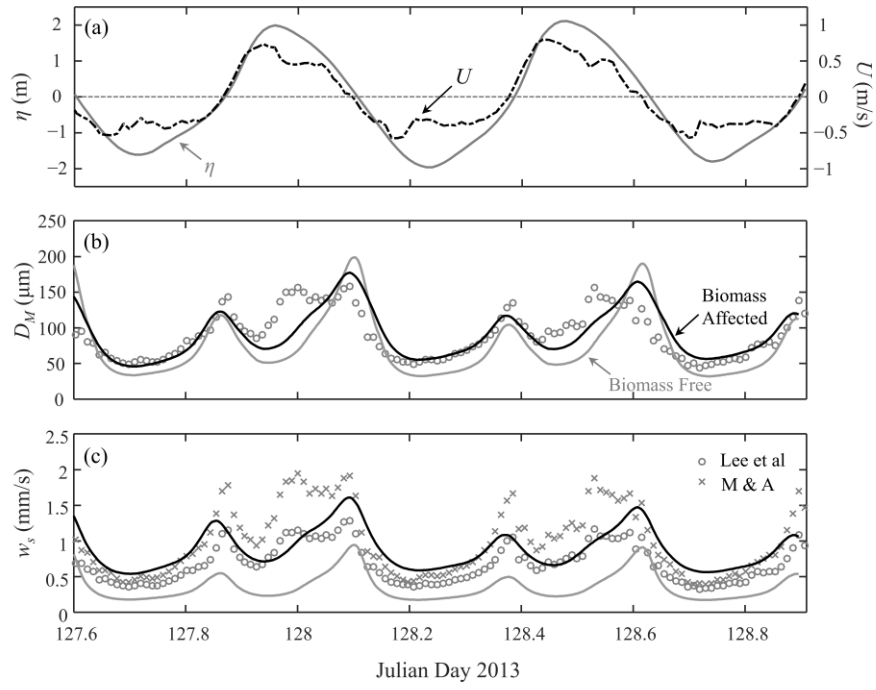


Fig. 9

ACCEPTED

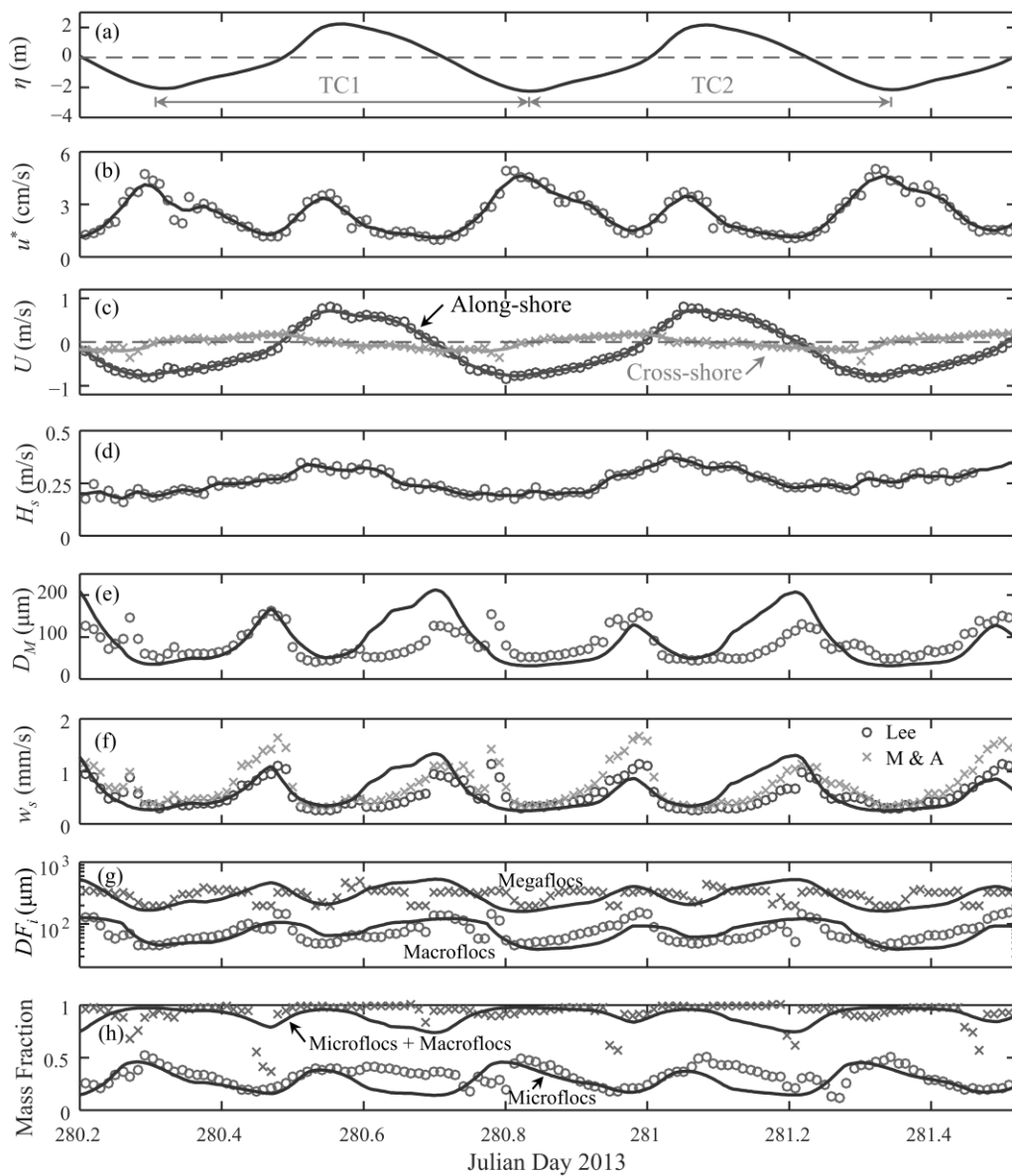


Fig. 10

Table 1 Aggregation and breakage processes of suspended particles with five tracers.

Processes (j) ↓	Description	Components (i) →					Creation Rate
		N_P	N_{F1}	N_{T1}	N_{F2}	N_{T2}	
(1) Aggregation <i>Microflocs & Microflocs</i>		$-\frac{1}{2} \left(\frac{N_{C1}}{N_{C1}-1} \right)$	$\frac{1}{2} \left(\frac{1}{N_{C1}-1} \right)$	$\frac{1}{2} \left(\frac{N_{C1}}{N_{C1}-1} \right)$	0	0	$\alpha \beta_{PP} N_P N_P$
(2) Aggregation <i>Microflocs & Macroflocs</i>		-1	0	+1	0	0	$\alpha \beta_{PF1} N_P N_{F1}$
(3) Aggregation <i>Microflocs & Megaflocs</i>		-1	0	0	0	+1	$\alpha \beta_{PF2} N_P N_{F2}$
(4) Aggregation <i>Macroflocs & Macroflocs</i>		0	$-\frac{1}{2} \left(\frac{N_{C2}/N_{C1}}{N_{C2}/N_{C1}-1} \right)$	$-\frac{1}{2} \left(\frac{N_{C2}}{N_{C2}/N_{C1}-1} \right)$	$\frac{1}{2} \left(\frac{1}{N_{C2}/N_{C1}-1} \right)$	$\frac{1}{2} \left(\frac{N_{C2}}{N_{C2}/N_{C1}-1} \right)$	$\alpha \beta_{F1F1} N_{F1} N_{F1}$
(5) Aggregation <i>Macroflocs & Megaflocs</i>		0	-1	$-N_{C1}$	0	N_{C1}	$\alpha \beta_{F1F2} N_{F1} N_{F2}$
(6) Aggregation <i>Megaflocs & Megaflocs</i>		0	0	0	$-\frac{1}{2}$	0	$\alpha \beta_{F2F2} N_{F2} N_{F2}$
(7) Breakage <i>Macroflocs</i>		$f_{P1} \cdot N_{C1}$	$K_1 - 1$	$-f_{P1} \cdot N_{C1}$	0	0	$a_{F1} N_{F1}$
(8) Breakage <i>Megaflocs</i>		$f_{P2} \cdot N_{C2}$	K_2	$(1-f_{P2}) \cdot N_{C2}$	-1	$-N_{C2}$	$a_{F2} N_{F2}$

Nomenclature: N_P = number of microflocs in suspension per unit volume; N_{F1} = number of macroflocs in suspension per unit volume; N_{F2} = number of megaflocs in suspension per unit volume; N_{T1} = number of microflocs in macroflocs per unit volume; N_{T2} = number of microflocs in megaflocs per unit volume; N_{C1} = number of microflocs in one macrofloc, $N_{C1} = N_{T1} / N_{F1}$; N_{C2} = number of microflocs in one megafloc, $N_{C2} = N_{T2} / N_{F2}$; f_{P1} = mass fraction of created microflocs when a macrofloc breaks up; f_{P2} = mass fraction of created microflocs when a megafloc breaks up; K_1 = number of created macroflocs when a parent macrofloc breaks up; K_2 = number of created macroflocs when a megafloc breaks up; α = collision efficiency; β_{PP} = collision frequency between two microflocs; β_{PF1} = collision frequency between a microfloc and a macrofloc; β_{PF2} = collision frequency between a microfloc and a megafloc; β_{F1F1} = collision frequency between two macroflocs; β_{F1F2} = collision frequency between a macrofloc and a megafloc; β_{F2F2} = collision frequency between two megaflocs; a_{F1} = breakup frequency of a macrofloc; a_{F2} = breakup frequency of a megafloc. The shaded is to emphasize the new tracer N_{F2} , compared with previous model by Shen et al. (2018).

Table 2 Parameters used in the best quality simulation at station MOW1 for algae bloom period.

Flocculation Kinetics	Value	Description
α	0.2	Collision efficiency
E_b	1.0×10^{-4}	Breakup fitting parameter
F_y	1.0×10^{-10}	Floc strength (Pa)
f_{P1}	0.2	Mass fraction of created microflocs when a macrofloc breaks up
f_{P2}	0.2	Mass fraction of created microflocs when a megafloc breaks up
K_1	1.5	Number of created macroflocs when a larger macrofloc breaks up
K_2	2	Number of created macroflocs when a megafloc breaks up
nf	2.3	Fractal dimension of suspended flocs
K_B	1.38×10^{-23}	Boltzmann constant (J/K)
T	283.0	Temperature (K)
r_B	2.0×10^{-5}	Growth rate of biomass (s^{-1})
Ω	0.047	Biomass fraction
γ_F	0.45	Coefficient in computing carrying capacity of microflocs
Initial Condition ($t = 0$)	Value	Description
c	0.2	Sediment mass concentration (g/L)
D_P	12	Size of microflocs (μm)
D_{F1}	100	Size of macroflocs (μm)
D_{F2}	300	Size of megaflocs (μm)
Ψ_P	10	Mass percentage of microflocs (%)
Ψ_{F1}	10	Mass percentage of macroflocs (%)
Ψ_{F2}	80	Mass percentage of megaflocs (%)
Other parameters	Value	Description
Δt	5	Time step (s)
n_z	12	Number of horizontal levels
τ_{ce}	1.0	Critical shear stress for erosion (Pa)
M	1.0×10^{-4}	Empirical erosion parameter ($\text{kg} \cdot \text{m}^{-2} \cdot \text{s}^{-1}$)
ρ_P	2200	Microfloc density ($\text{kg} \cdot \text{m}^{-3}$)
ρ_w	1024	Sea water density ($\text{kg} \cdot \text{m}^{-3}$)

Highlights

- The biomineral flocs in the Belgian coast were investigated during two contrasting periods;
- The observed floc size distributions were decomposed to represent microflocs, macroflocs and megaflocs;
- A simple flocculation model that can describe the biofilm growth of flocs was developed;
- This model was successfully implemented in the open TELEMAC with five passive tracers.

ACCEPTED MANUSCRIPT